ELSEVIER

# Contents lists available at ScienceDirect

# Chemical Geology

journal homepage: www.elsevier.com/locate/chemgeo





# Source variations in volatile contents of Bransfield Strait back-arc and Phoenix/West Scotia mid-ocean ridge lavas, northern Antarctic Peninsula

D.W. Anderson <sup>a,\*</sup>, A.E. Saal <sup>a</sup>, S. Mallick <sup>a</sup>, J. Wang <sup>b</sup>, T.R. Riley <sup>c</sup>, R.A. Keller <sup>d</sup>, K.M. Haase <sup>e</sup>

- <sup>a</sup> Department of Earth, Environmental and Planetary Sciences, Brown University, Providence, RI 02912, USA
- <sup>b</sup> Earth and Planets Laboratory, Carnegie Institution for Science, Washington, DC 20015, USA
- <sup>c</sup> British Antarctic Survey, High Cross, Madingley Road, Cambridge CB3 0ET, UK
- <sup>d</sup> College of Earth, Oceanic and Atmospheric Sciences, Oregon State University, Corvallis, OR 97331, USA
- e GeoZentrum Nordbayern, Universität Erlangen-Nürnberg, Schloßgarten 5, D-91054 Erlangen, Germany

#### ARTICLE INFO

#### Editor: Marco Fiorentini

Original content: Data for: Source variations in volatile contents of Bransfield Strait back-arc and Phoenix/West Scotia mid-ocean ridge lavas, northern Antarctic Peninsula (Original data)

Keywords: Volatiles Subduction Back-arc basin Bransfield Strait Phoenix Ridge

#### ABSTRACT

We present the first volatile contents  $(H_2O,CO_2,Cl,F,S)$  of young  $(<6\,Ma)$  submarine basaltic glasses from the Phoenix and West Scotia mid-ocean ridges and the Bransfield Strait back-arc of the South Shetland subduction zone in the Antarctic Peninsula.

The volatile contents of the MORB glasses correspond well with those of published Pacific MORB and reflect covariations in source enrichment and extent of melting. Our results support the hypothesis that decreasing spreading rates at the Phoenix Ridge resulted in preferential melting of less abundant enriched MORB mantle, due to its greater fertility and higher volatile contents, relative to the more abundant depleted MORB mantle.

The volatile contents of the Bransfield Strait back-arc glasses correlate with geochemical indicators of subduction processes and reveal an along-axis spatial distribution consistent with a toroidal inflow of sub-slab asthenosphere around the edges of the subducting plate into the mantle wedge. This inflow should be considered when assessing spatial and geochemical variability at subduction zones, particularly those with slab windows and tears.

A small group of Bransfield Strait samples have volatile contents that do not correlate with geochemical signals of subduction influence. We speculate that these samples reflect flux melting of residual enriched mantle brought beneath the Bransfield Strait via corner flow following recent alkaline magmatism in the far eastern regions of the Antarctic Peninsula.

Our new data on lavas from the W7 segment of the West Scotia Ridge reveal their source was significantly affected by subduction processes. Unexpectedly, these lavas have  $CO_2$ - $H_2O$  pressures of vapor saturation that suggest they were collected in-situ and erupted relatively recently ( $\sim$ 6 Ma), at odds with previous interpretations of their origins. We suggest they originated from a subduction-modified mantle (lithosphere or asthenosphere) left behind by the eastward-migrating South Sandwich subduction zone sometime over the past  $\sim$ 30 Myr. These lavas demonstrate the long-lasting effects of subduction processes on the upper mantle and their potential to influence melt compositions even in non-subduction environments today.

We use the compositions of lavas from the Phoenix Ridge and Bransfield Strait to estimate mantle potential temperatures; our results agree well with global estimates for mid-ocean ridges and subduction zones, respectively.

# 1. Introduction

Volatiles have strong effects on mantle melting and magma crystallization, especially at subduction zones where there is a heavy supply of fluids from the subducting slab (e.g., Stolper and Newman, 1994; Wallace, 2005). Along-slab variations in fluid flux have been used to explain spatial trends in the geochemistry of arc and back-arc lavas at subduction zones across the world, but often these studies are not supplemented with volatile data (e.g., Pearce et al., 2005; Barry et al., 2006; Haase et al., 2012). Submarine glasses from along the length of the

E-mail address: danny\_anderson@brown.edu (D.W. Anderson).

https://doi.org/10.1016/j.chemgeo.2023.121839

<sup>\*</sup> Corresponding author.

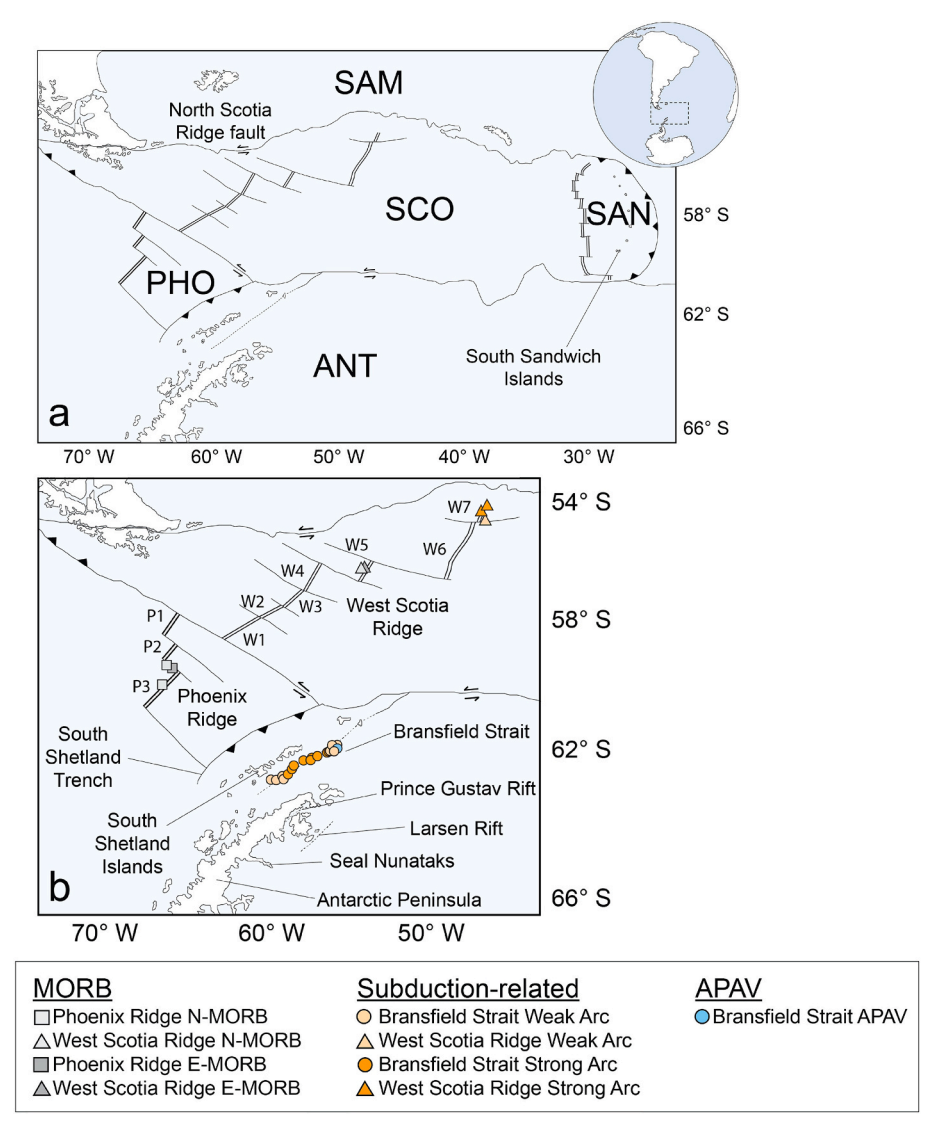


Fig. 1. a) Map of the greater Antarctic Peninsula region showing the positions of the South American (SAM), Phoenix (PHO), Antarctic (ANT), Scotia (SCO), and Sandwich plates (SAN). Also pictured are the North Scotia Ridge fault and the South Sandwich Islands volcanic front of the South Sandwich subduction zone. b) Map of the northern Antarctic Peninsula, showing the locations of the Phoenix and West Scotia mid-ocean ridges, the South Shetland trench, the South Shetland Islands volcanic front, the Seal Nunataks, and the Bransfield Strait, Prince Gustav Rift, and Larsen Rift back-arcs. Individual segments of the Phoenix (P1-P3) and West Scotia (W1-W7) ridges are also labeled. Dredge locations for samples from this study are marked by circles in the Bransfield Strait, squares in the Phoenix Ridge, and triangles in the West Scotia Ridge. Symbol colors correspond to the representative geochemistry of samples from each dredge.

Bransfield Strait, a back-arc of the South Shetland subduction zone in the northern Antarctic Peninsula, are ideal samples to investigate trenchparallel variations in fluid flux. Their major and trace element contents and radiogenic isotope compositions indicate significant alongtrench differences in the extent of slab-derived material fluxing the mantle wedge (e.g., Fretzdorff et al., 2004; Anderson et al., 2023). The abundant glassy rinds from basalts erupted at 1-2 km depth below the sea surface make excellent targets to measure volatile concentrations (Stolper and Newman, 1994; Dixon and Stolper, 1995; Shimizu et al., 2016). Furthermore, we have the advantage of using geochemically well-characterized basalts from the nearby Phoenix and West Scotia mid-ocean ridges to infer a local "background" mantle composition unaffected by subduction processes. Here we present the first volatile measurements (H2O, CO2, Cl, F, S) of submarine glasses from the Bransfield Strait, Phoenix Ridge, and West Scotia Ridge to assess the volatile contents of mantle sources beneath the ridges and the trenchparallel variability in the slab flux throughout the South Shetland subduction zone mantle wedge.

# 2. Geologic background

# 2.1. The South Shetland subduction zone

Since the Mesozoic, ongoing subduction of the Phoenix Plate beneath the Antarctic Plate has shaped the geologic history of the Antarctic Peninsula (Fig. 1). This subduction zone is characterized by the South Shetland Islands volcanic front and a series of back-arc extensional features at progressive distances from the trench: The Bransfield Strait, the Prince Gustav Rift, and the Larsen Rift. Our study is centered on the Bransfield Strait, where recent submarine volcanism offers a unique opportunity to study the effects of subduction processes on the mantle of the northern Antarctic Peninsula. The limits of the Bransfield Strait roughly coincide with the modern extent of the trench, leading many workers to suggest that the strait opened through lithospheric thinning in response to roll-back of the subducting Phoenix slab in recent (<4 Ma) times (e.g., Barker, 1982; Haase and Beier, 2021). Today, seismic evidence suggests that the South Shetland subduction zone remains active, though subduction is proceeding quite slowly (Jordan et al., 2020; Leat

Chemical Geology 646 (2024) 121839

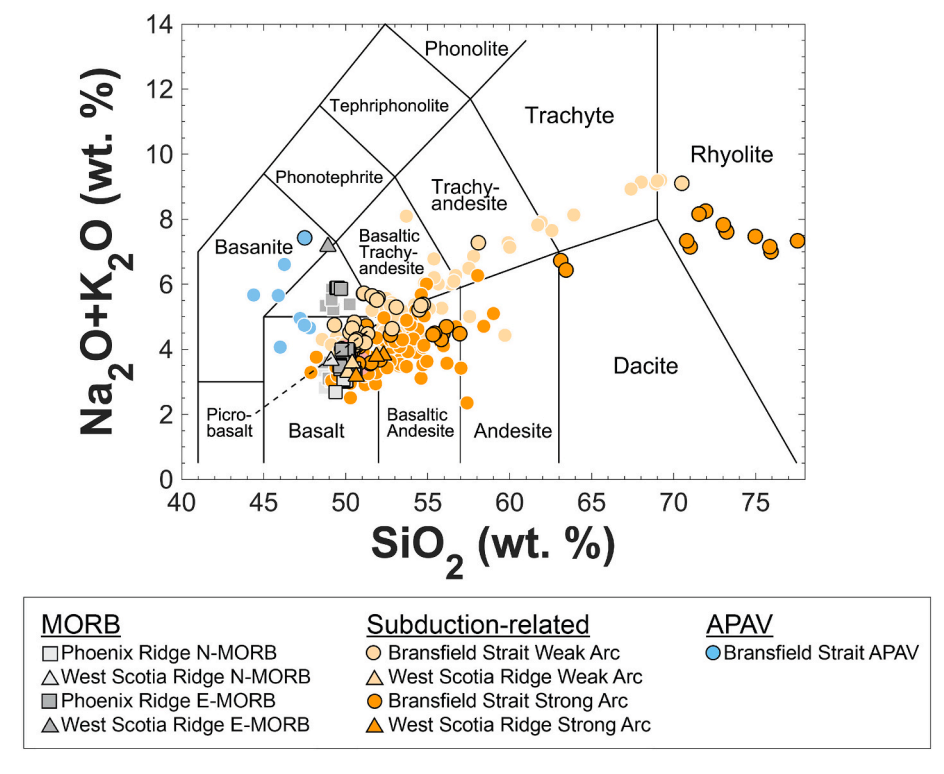


Fig. 2. Total alkalis vs silica diagram showing the compositions of the lavas from Anderson et al. (2023) used in this study, which are marked with black borders. Borderless symbols are published data from the Phoenix Ridge (Haase et al., 2011) and the Bransfield Strait (Baker et al., 1975; Weaver et al., 1979; Keller et al., 1992; Keller and Fisk, 1992; Keller et al., 2002; Fretzdorff et al., 2004; Kraus et al., 2013; Martí et al., 2013). The APAV (Antarctic Peninsula Alkaline Volcanic) group represents alkaline melts with unique isotope ratios and no clear subduction signals in their trace element compositions. Dashed line represents the alkaline-subalkaline boundary from MacDonald and Katsura (1964).

and Riley, 2021a, 2021b).

# 2.2. The Phoenix and West Scotia ridges

Neighboring the South Shetland subduction zone are the Phoenix and West Scotia mid-ocean ridges (Fig. 1). The lavas from these areas are important points of comparison for our study since they sample a portion of the upper mantle that has not been modified by subduction processes, with the exception of lavas from the West Scotia Ridge segment W7. The three segments of the Phoenix Ridge are what remain today of an extensive mid-ocean ridge system that was progressively consumed during a series of collisions with the trench from ~50-4 Ma (Barker, 1982; Hole et al., 1994; Hole, 2021). The oblique angle between the trench and ridge segments resulted in the formation of a slab window beneath the Antarctic Peninsula from southwest to northeast, as the trailing half of each segment remained locked at the trench while the leading half continued to subduct (Hole, 1990; Guenthner et al., 2010; Hole, 2021). Spreading rates at the ridge decreased significantly until extreme slowdown by 3.3 Ma, though published ages for samples collected along and near the ridge axis range to as young as 1 Ma (Livermore et al., 2000; Choe et al., 2005; Choi et al., 2008; Haase et al., 2011).

Spreading at the West Scotia Ridge initiated  $\sim 30$  Ma, resulting in the eastward opening of the Drake Passage and formation of the Central Scotia Plate (predecessor to today's Scotia Plate), north of the Antarctic Peninsula (Eagles, 2010; Maldonado et al., 2014; Fig. 1). The seven segments of the West Scotia Ridge continued spreading until extinction  $\sim 6$  Ma (Eagles et al., 2005; Maldonado et al., 2014).

# 3. Materials and methods

For each sample, three to five hand-picked chips of the freshest

available, naturally-quenched submarine volcanic glass were mounted in indium and polished using diamond grit paste down to 1  $\mu m.$  Additionally, a small subset of olivine phenocrysts from six samples were mounted, polished, and analyzed for their major element and V concentrations to estimate Fe $^{3+}/\text{Fe}_{T}$  following the approach of Kelley and Cottrell (2012). Multiple glass chips and olivine separates were used per sample to characterize natural variation of the sample and determine the reproducibility of the measurement. Wherever possible, measurements were made on the glass encompassing the olivine separates, though not all olivine grains were directly in contact with analyzable glass.

All new data are reported in Supplementary Tables S1-S3 and through Mendeley Data at https://doi.org/10.17632/stz3xzt98n.1. The major and trace element concentrations and isotope ratios of most lavas used in this study were previously reported by Anderson et al. (2023). However, we re-collected major element and V concentrations for several samples with glass in contact with the olivine separates, which we used to estimate their Fe<sup>3+</sup>/Fe<sub>T</sub> (Kelley and Cottrell, 2012). In addition, we present new data for six lavas from the W7 segment of the West Scotia Ridge analyzed during the same analytical sessions as the data reported in Anderson et al. (2023) but never published. These six samples were dredged during the British Antarctic Survey cruise JR16003 (November 2016-January 2017) on RRS James Clark Ross, and the dredge locations for all samples are listed in Supplementary Table S2 and shown in Fig. 1. We also report new isotope ratios for three Bransfield Strait lavas with previously published major and trace element data from Anderson et al. (2023). Their material was provided by the Polar Rock Repository (PRR), Byrd Polar and Climate Research Center (BPCRC), Ohio State University. Finally, we report data for one basaltic sample from the Seal Nunataks, R3723.7 (collected by the British Antarctic Survey; Fig. 1), which we use for the model in Supplementary Fig. S1. Major and trace element contents were measured on whole rock powder at the Peter Hooper GeoAnalytical Lab at Washington State

Chemical Geology 646 (2024) 121839

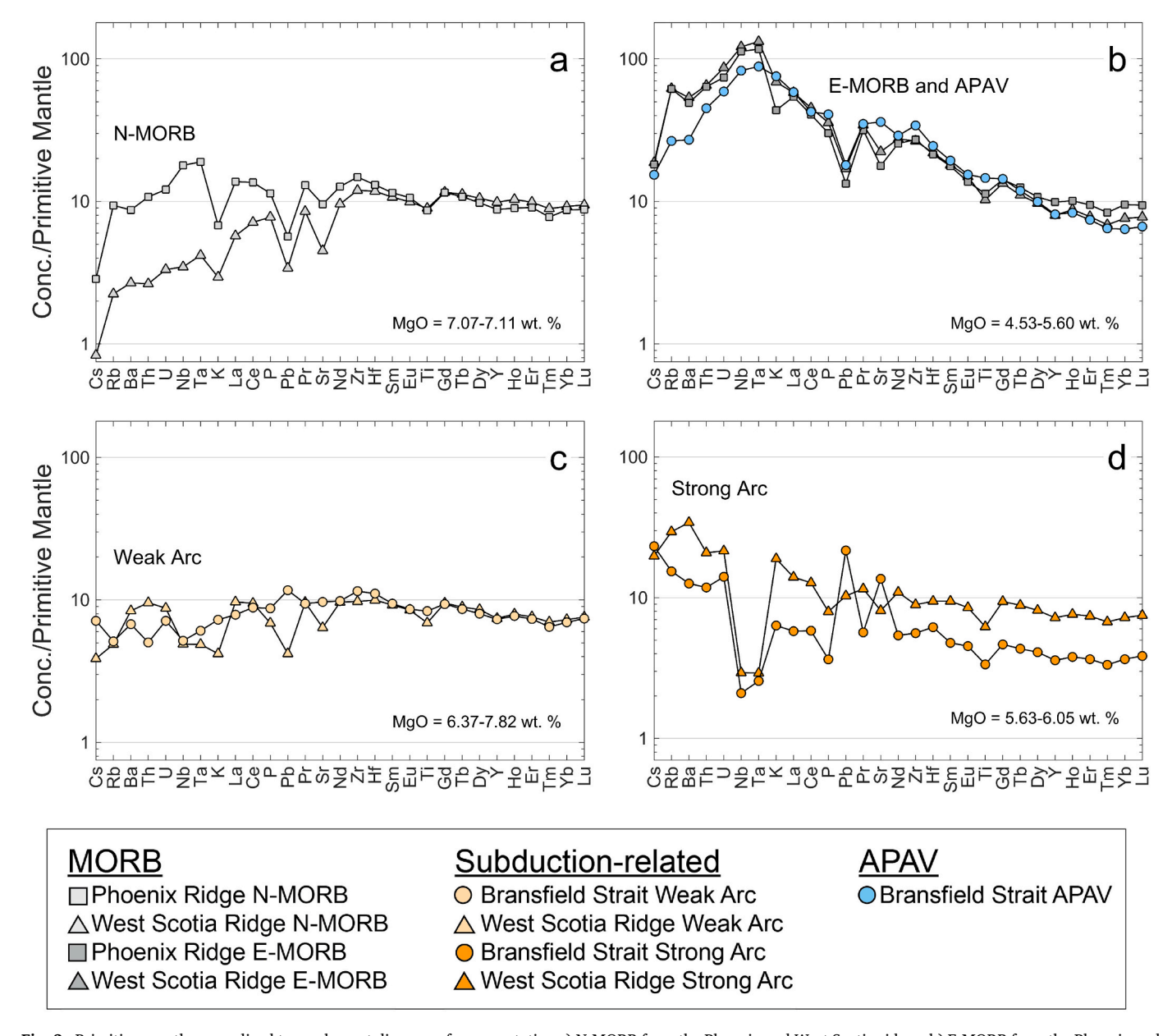


Fig. 3. Primitive mantle normalized trace element diagram of representative a) N-MORB from the Phoenix and West Scotia ridges, b) E-MORB from the Phoenix and West Scotia ridges and APAV from the Bransfield Strait, c) Weak Arc lavas from the Bransfield Strait and West Scotia Ridge, and d) Strong Arc lavas from the Bransfield Strait and West Scotia Ridge. Primitive mantle composition is from McDonough and Sun (1995).

University (see lab for details on long term precision and standards: https://environment.wsu.edu/facilities/geoanalytical-lab). A detailed description of how all major and trace element and isotope analyses were conducted is provided in Anderson et al. (2023), and we present abbreviated methods below.

Volatile element ( $H_2O$ ,  $CO_2$ , Cl, F, and S) analyses were performed using the Cameca 6F ion probe at the Carnegie Institution for Science. Each glass chip was analyzed using a 10–15 nA current, 10 µm diameter  $Cs^+$  primary beam scanned over a 20 µm diameter raster area using a manual diaphragm to avoid surface contamination. Data come from a 3 µm circle within this area. Spots were pre-sputtered for 180 s prior to 210 s count times. See Hauri et al. (2002) for further details on analytical techniques and standards. Reproducibility of the three to five chips for each individual sample was calculated, then averaged across all samples. For the Phoenix and West Scotia Ridge glasses, the average reproducibility ( $2\sigma$  SE) is < 5% for all volatiles except  $CO_2$  and Cl, which are < 8%. For Bransfield Strait glasses, the average reproducibility ( $2\sigma$  SE) is <

8% for all volatiles except  $CO_2,$  which is  $\sim 24\%$  on account of extremely low concentrations. Average root mean square errors on our volatile calibration curves were <5% for Cl, <6% for F, <9% for CO<sub>2</sub>, and <10% for S and  $H_2O$ .

Major element analyses for the glasses and olivine separates were performed on the Brown University Cameca SX-100 electron microprobe. The operating conditions of the instrument consisted of 15 kV voltage, 10 nA current and either a 10  $\mu m$  (glass) or a 1  $\mu m$  (olivine) diameter spot size. Reproducibility of repeated analyses per sample was calculated, then averaged across all samples. For the glasses, the average reproducibility (2 $\sigma$  SE) for each oxide is <0.5% for SiO2, <1% for Al2O3 and FeOT, <1.6% for MgO and CaO, <2.8% for TiO2 and Na2O, <5.5% for K2O, <10.5% for P2O5, and <14.5% for MnO, consistent with values reported in Anderson et al. (2023). For the olivine, the average reproducibility (2 $\sigma$  SE) is, <0.5% for SiO2 and MgO, 1.75% for FeO, and <10.5% for MnO. To ensure the olivine was in equilibrium with its surrounding glass, we calculated molar Mg# for each grain, as Mg/(Mg +

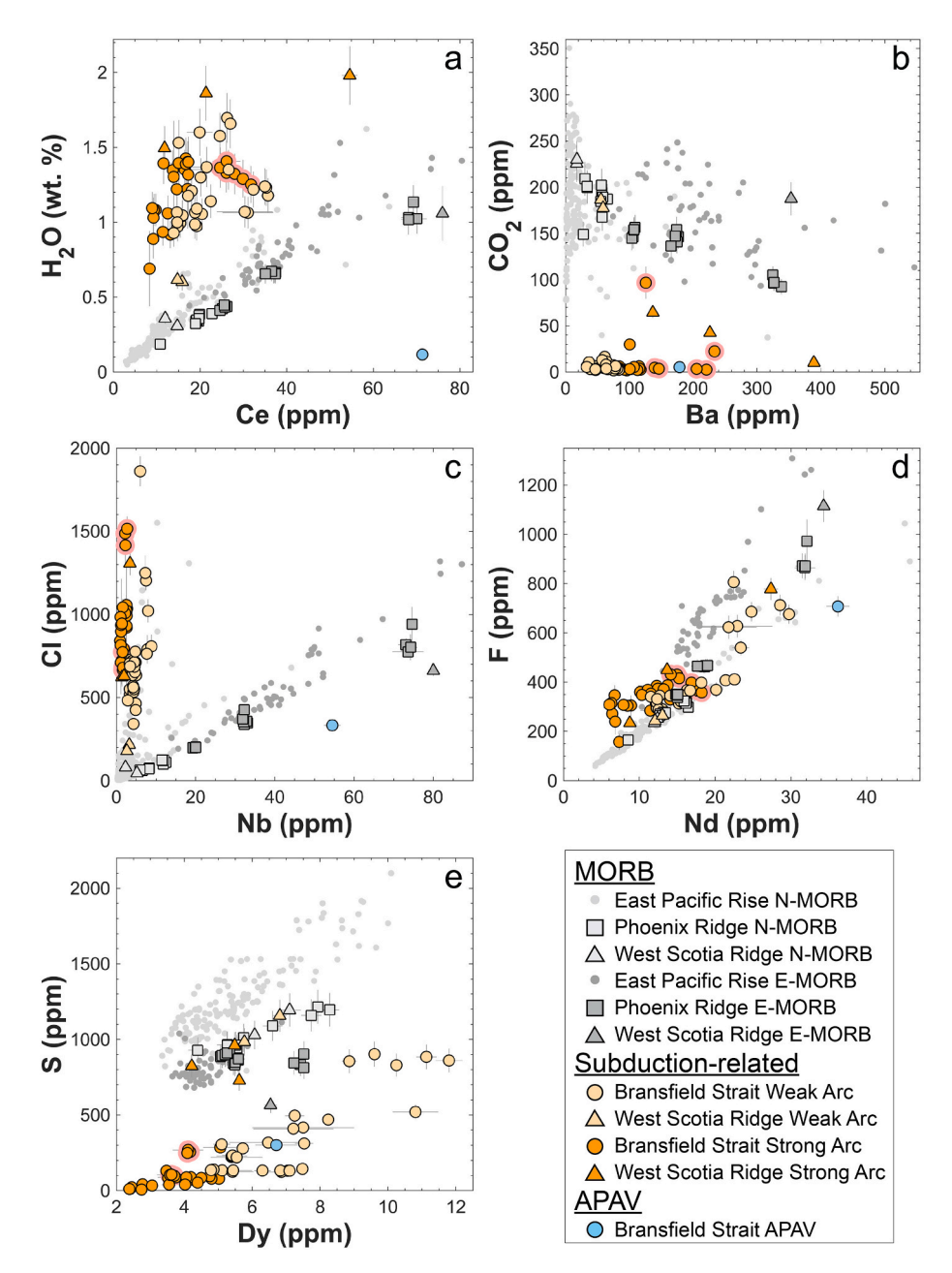


Fig. 4. Variations in volatile contents vs refractory trace elements of similar incompatibility during mantle melting. a)  $H_2O$  vs Ce, b)  $CO_2$  vs Ba, c) Cl vs Nb, d) F vs Nd, e) S vs Dy. Error bars reflect each sample's  $2\sigma$  standard error for each element. In cases where the volatile calibration error was larger than the standard error, that was used instead. Small gray circles here and in subsequent figures are published Pacific MORB from the East Pacific Rise (Shimizu et al., 2016). Dark gray represents E-MORB (Th/La > 0.11) and light gray represents D- and N-MORB (Th/La < 0.11). Pacific MORB data here are not filtered for assimilation of hydrothermally altered crust and brines. Pink highlighted Strong Arc samples from the Bransfield Strait here and in subsequent figures represent Strong Arc lavas with incompatible trace element patterns distinct from other Bransfield Strait lavas. See Section 5.2.2 for details and discussion. All data here and in subsequent figures are filtered for MgO > 3.0 wt%. (For interpretation of the references to color in this figure legend, the reader is referred to the web version of this article.)

Fe<sup>2+</sup>), and then we compared that value to the Mg# of olivine that would be in equilibrium with the glass using an olivine-melt Fe<sup>2+</sup>/Mg K<sub>D</sub> of 0.3 (Roeder and Emslie, 1970). The reproducibility of secondary standards USGS BCR-2G and San Carlos Fo90 olivine is <1% (2 $\sigma$  SE) for all major elements except MnO (5.4%).

Trace element concentrations of glasses and V contents of olivine separates were determined by 193 nm wavelength excimer Analyte G2 laser ablation system coupled to a Thermo Scientific X-Series II quadrupole ICP-MS at Brown University. Olivine separates were analyzed using a 150  $\mu$ m spot with a 20 Hz repetition rate and a laser frequency of 3.78 J/cm² at 50% energy level. Glass chips were analyzed using a 150  $\mu$ m spot and 10 Hz repetition rate, though for some partially crystallized

or vesiculated samples, the spot size was reduced to 85  $\mu m$ . The average reproducibility (2 $\sigma$  SE) obtained for the glass samples is better than 8%, consistent with values reported in Anderson et al. (2023).

The new isotope data reported here were collected on hand-picked glass chips that were leached with cold 2.5 N HCl for 30 min, dissolved in a mixture of HF(3):HNO<sub>3</sub>(1), and then processed through ion exchange chromatography. Sr, Nd, Hf, and Pb isotopic compositions were measured on a Thermo Scientific Neptune Plus MC-ICP-MS at the Mass Spectrometer Analytical Facility, Brown University. To account for instrumental mass fractionation, we applied corrections using  $^{86} {\rm Sr}/^{88} {\rm Sr} = 0.1194, \, ^{146} {\rm Nd}/^{144} {\rm Nd} = 0.7219$  and  $^{179} {\rm Hf}/^{177} {\rm Hf} = 0.7325$  and an exponential law. Sample Pb solutions were spiked with NBS SRM-997 Tl

Chemical Geology 646 (2024) 121839

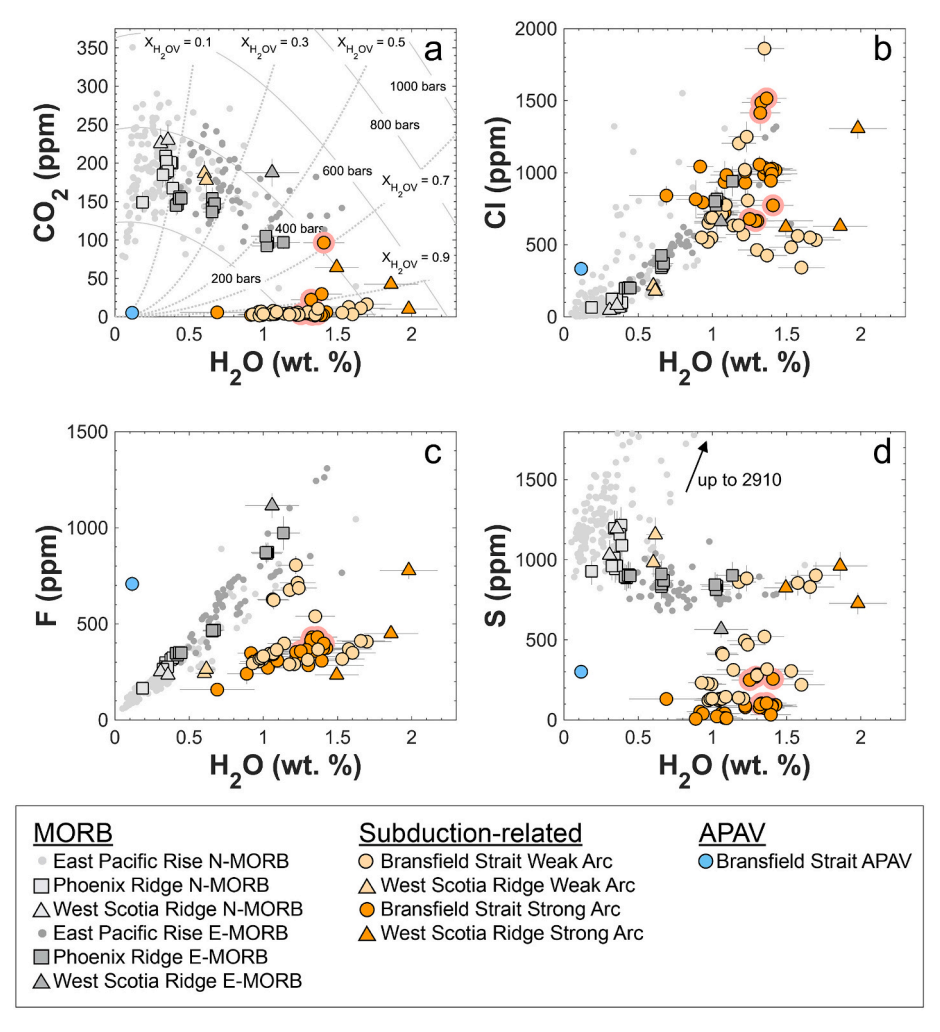


Fig. 5. Variations in a) CO<sub>2</sub>, b) Cl, c) F, and d) S vs H<sub>2</sub>O in the northern Antarctic Peninsula submarine glasses and Pacific MORB (not filtered for assimilation of hydrothermally altered crust and brines; Shimizu et al., 2016). Error bars reflect each sample's 2σ standard error for each volatile element. In cases where the volatile calibration error was larger than the standard error, that was used instead. Isobars and isopleths in a) were calculated for the composition of tholeitic N-MORB sample 53DR-20 with the VESIcal web-app (v 1.0.1; Iacovino et al., 2021) using the model of Ghiorso and Gualda (2015) at 1200 °C.

standard prior to analysis with a Pb/Tl ratio of ~4 to correct for mass fractionation using an exponential law and  $^{203}\text{Tl}/^{205}\text{Tl}=0.418922.$  Sr, Nd, and Hf isotope ratios are reported relative to NBS SRM-987  $^{87}\text{Sr}/^{86}\text{Sr}=0.71024,$  JNd-i  $^{143}\text{Nd}/^{144}\text{Nd}=0.512115,$  and JMC-475  $^{176}\text{Hf}/^{177}\text{Hf}=0.282160,$  respectively. Pb isotope ratios are reported relative to the NBS 981  $^{206}\text{Pb}/^{204}\text{Pb}=16.9356,$   $^{207}\text{Pb}/^{204}\text{Pb}=15.4891,$  and  $^{208}\text{Pb}/^{204}\text{Pb}=36.7006$  (Todt et al., 1996). The external precision on the ratios over the course of two years is 30 ppm for Sr (2\$\sigma\$) and Nd (2\$\sigma\$), 40 ppm for Hf (2\$\sigma\$) and 80 ppm (2\$\sigma\$) for Pb. All blanks were < 50 pg.

# 4. Results

We report new volatile data for a suite of lavas that were previously analyzed for major and trace element contents, and isotope ratios (Anderson et al., 2023). Additionally, we report new major element, trace element, and radiogenic isotope compositions for a set of West Scotia Ridge lavas from the northernmost W7 segment. The lavas in this study extend in composition from basaltic to rhyolitic and range from tholeitic to slightly alkalic, though there are a few instances of trachybasalts and basanites (Fig. 2). Isotope data on the most differentiated samples from the Bransfield Strait overlap with the range of more primitive lavas from the same area, suggesting that crustal assimilation is not controlling their compositions (Anderson et al., 2023). However, to avoid the effects of accessory mineral crystallization on the volatile/

refractory incompatible trace element ratios used in this study, we do not consider data for any sample more differentiated than basaltic andesite when assessing source variations in volatile contents. All data and results are presented in Fig. 2 and Supplementary Table S2, but in all other figures the data are filtered for  $SiO_2 < 57.0$  wt%.

We separate the samples into four groups based on tectonic setting, source enrichment, and extent of subduction influence (Fig. 3). We assess the effects of subduction using ratios of fluid-mobile large ion lithophile elements (LILE; e.g., Cs, Rb, Ba, K) to fluid-immobile high field strength elements (HFSE; e.g., Nb, Ta) (e.g., Rustioni et al., 2021). These ratios are hereafter referred to as "subduction signal." We also include Th/La, since increases in this ratio indicate sediment input into the source of arc and back-arc lavas (Johnson and Plank, 2000; Plank, 2005). Surprisingly, subduction signals have been reported in lavas from the W7 segment of the West Scotia Ridge, and our new data corroborate that these melts have been affected by a subduction-like source (Riley et al., 2019; Fig. 3c–d). We add these new West Scotia Ridge lavas to the appropriate compositional groups, described below, according to the strengths of their subduction signals.

The four main compositional groups, which come from Anderson et al. (2023), are defined as follows. 1) *MORB* from the Phoenix and West Scotia ridges, which have compositions consistent with published Pacific MORB (Haase et al., 2011; Stracke, 2012; Anderson et al., 2023). This group forms a compositional range from normal MORB (N-MORB,

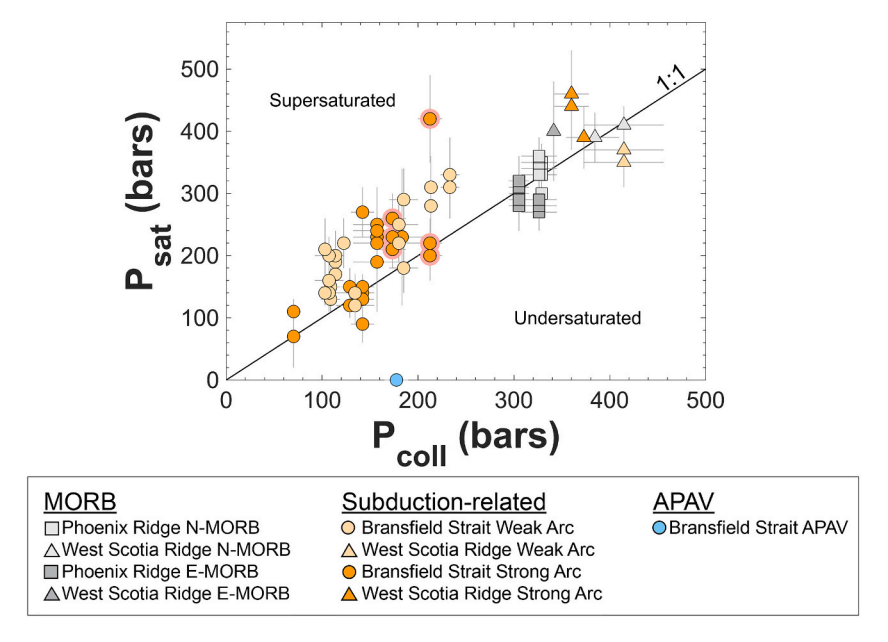


Fig. 6. Modeled pressure of saturation ( $P_{sat}$ ) vs pressure of collection ( $P_{coll}$ ) for our samples.  $P_{sat}$  values calculated with the VESIcal web-app (v 1.0.1; Iacovino et al., 2021) using the model of Ghiorso and Gualda (2015) at 1200 °C.  $P_{coll}$  values were calculated using the average depth of each dredge. Vertical errors were calculated by propagating the uncertainties of our  $H_2O$  and  $CO_2$  measurements through the model, though this does not account for errors in the model itself. Horizontal errors are calculated using the variation in depth for each dredge. Symbols plotting above, on, and below the 1:1 line represent  $CO_2$ - $H_2O$  supersaturated, saturated, and undersaturated lavas at their pressures of collection, respectively.

0.06 < Th/La < 0.11, after Shimizu et al., 2016) to enriched MORB (E-MORB, Th/La > 0.11). 2) Weak Arc lavas from the Bransfield Strait and West Scotia Ridge, which have weak subduction signals (Fretzdorff et al., 2004; Riley et al., 2019; Anderson et al., 2023). 3) Strong Arc lavas from the Bransfield Strait and West Scotia Ridge, which have the strongest subduction signals (Fretzdorff et al., 2004; Riley et al., 2019; Anderson et al., 2023). We note that the cutoff between Weak and Strong Arc is arbitrary —lavas of both groups form a spectrum of increasing subduction signal that extends from MORB. 4) Antarctic Peninsula Alkaline Volcanic lavas (APAV), which are seemingly ubiquitous alkaline lavas found across the region that carry no clear subduction signals (e.g., Hole, 1990; Košler et al., 2009; Hole, 2021; Panter et al., 2022; Anderson et al., 2023). We were only able to retrieve glass and measure the volatile contents of one APAV submarine sample from the Bransfield Strait.

The samples show wide variations in volatile contents; in Fig. 4 we compare them to concentrations of refractory elements of similar incompatibility during mantle melting. In most cases, the MORB and arclike lavas define their own respective fields and slopes in these plots. Volatile contents roughly correlate with incompatible trace element enrichment in the MORB samples. The most trace element enriched MORB have the highest concentrations of H<sub>2</sub>O, Cl, and F and the lowest concentrations of CO<sub>2</sub> and S (Fig. 4-5). In the Bransfield Strait, Strong Arc lavas range to lower F and S than Weak Arc lavas, whereas the ranges in H<sub>2</sub>O, CO<sub>2</sub>, and Cl contents overlap between the two groups. Furthermore, nearly all Bransfield Strait lavas have extremely low CO2 contents, suggesting loss during magma degassing. Separations between West Scotia Weak and Strong Arc lavas are clearer than for the Bransfield Strait. West Scotia Strong Arc lavas range to greater abundances of H<sub>2</sub>O, Cl, and F and lower concentrations of CO<sub>2</sub> and S than Weak Arc lavas. Notably, West Scotia Ridge Weak Arc lavas largely have volatile concentrations within the range of N-MORB. The APAV sample has exceptionally low concentrations of H<sub>2</sub>O and CO<sub>2</sub> and relatively low Cl, F, and S contents compared to E-MORB samples from the Phoenix and West Scotia ridges.

#### 5. Discussion

# 5.1. The effect of shallow level processes on volatile contents

Past work has shown that the bulk partition coefficients of volatile elements are similar to certain refractory incompatible trace elements during mantle melting: H<sub>2</sub>O-Ce, CO<sub>2</sub>-Ba, Cl-K-Nb-Ba, F-Nd-P, S-Dy (e.g., Michael and Cornell, 1998; Danyushevsky et al., 2000; Saal et al., 2002; Rosenthal et al., 2015; Shimizu et al., 2016). By closely comparing variations in absolute volatile concentrations, ratios of volatile to refractory incompatible trace elements, and experimentally derived thermodynamic models, we can account for the effects of shallow level processes (e.g., crystal fractionation, magma degassing, contamination, assimilation of hydrothermally altered crust, sulfide saturation, etc.) and assess source variations in volatile abundance.

# 5.1.1. Crystal fractionation

Though we report data for andesites and rhyolites, they cannot be used reliably to assess source composition. This is due to the potential effects of late-stage crystallization of accessory minerals on the volatile/refractory trace element ratios of the glasses, making the ratios unreliable source indicators. Additionally, ratios of volatile elements themselves can be influenced by this differentiation process. For instance, Cl/F ratios, commonly used to distinguish between MORB and subduction influenced compositions can be modified by apatite fractionation during late stage crystallization. Thus, we do not consider these samples when assessing source variations in the upcoming discussion.

# 5.1.2. Degassing

A growing number of studies have shown the significant control that melt composition, exsolved gas composition, pressure,  $fO_2$ , etc. have on the solubility of volatiles and the extent to which degassing governs melt volatile composition, even at submarine pressures (e.g., Dixon, 1997; Straub and Layne, 2003; Wallace, 2005; Edmonds et al., 2009; Plank et al., 2013; Ghiorso and Gualda, 2015; Thomas and Wood, 2021; Hughes et al., 2023; Wieser et al., 2022; Ding et al., 2023). Thus, it is necessary to assess the effects of degassing on the volatile compositions

D.W. Anderson et al.

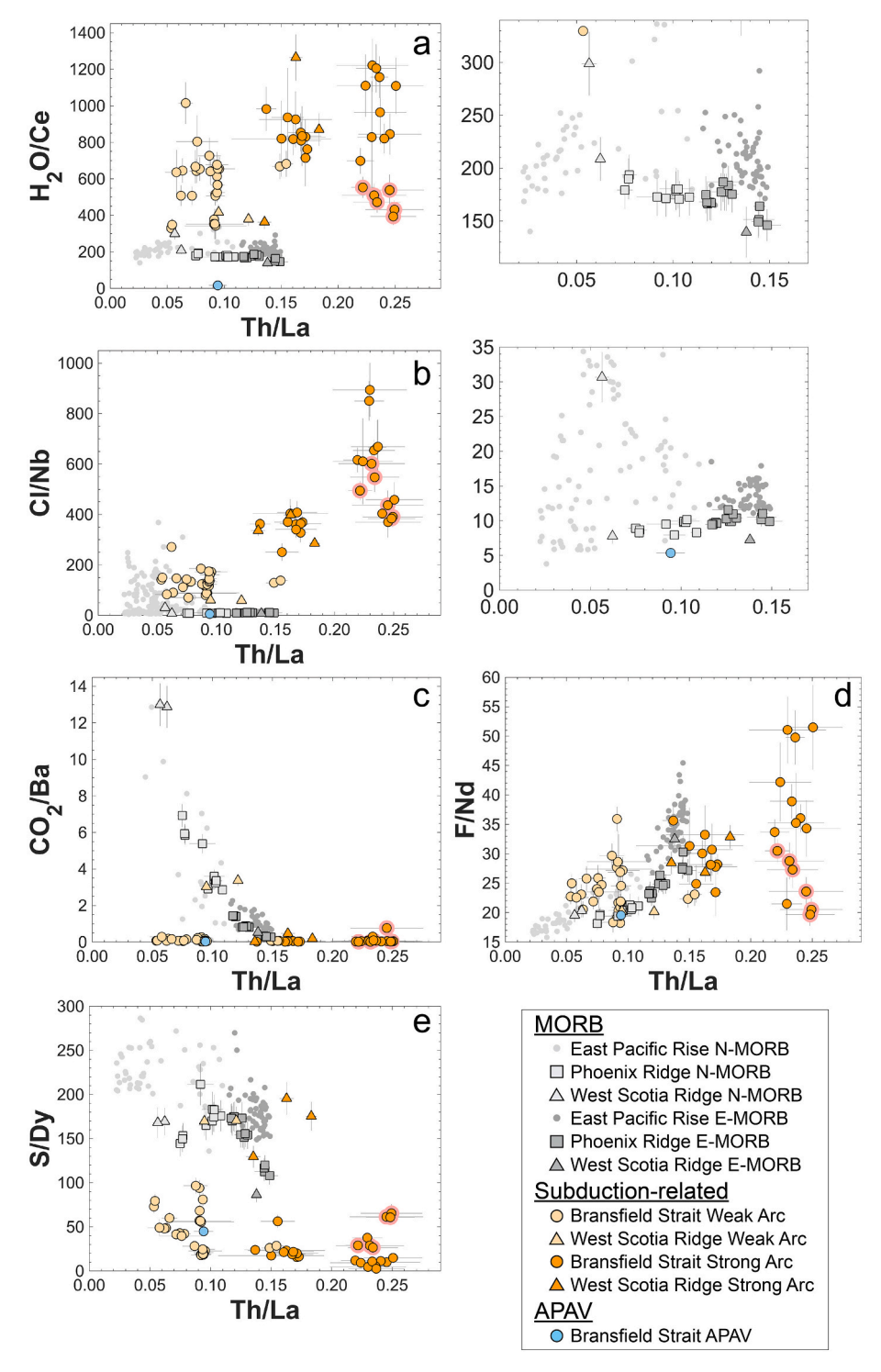


Fig. 7. a)  $H_2O/Ce$ , b) Cl/Nb, c) CO<sub>2</sub>/Ba, d) F/Nd, and e) S/Dy vs Th/La. Insets in a) and b) show expanded views of variations in  $H_2O/Ce$  and Cl/Nb, respectively, for our MORB compared to Pacific MORB (Shimizu et al., 2016). Pacific MORB data in all panels except b) are filtered for assimilation of hydrothermally altered crust and brines. Errors for each ratio are propagated from each sample's  $2\sigma$  standard error for each element. In cases where the volatile calibration error was larger than the standard error, that was propagated instead.

of the lavas. Using the compositions of the lavas in this study and the MagmaSat model of Ghiorso and Gualda (2015), we calculated pressures of  $CO_2$ - $H_2O$  saturation ( $P_{sat}$ ). We then compared these pressures to the approximate pressures of sample collection,  $P_{coll}$ , to assess whether the samples were  $CO_2$ - $H_2O$  saturated at their collection depths (Fig. 6). In nearly all cases, the lavas fall along the 1:1 line, indicating that they were saturateed at their collection depths (i.e., they were likely collected in-situ) and experienced some degree of  $CO_2$ - $H_2O$  degassing. A few

samples from the Bransfield Strait are  $CO_2$ - $H_2O$  supersaturated, with  $P_{sat}$  values above the 1:1 line. These samples must have ascended from within the crust so quickly that they failed to re-equilibrate prior to erupting. On average, this supersaturation corresponds to crustal depths of  $\sim\!270\,$  m, assuming a crustal density of 2800 kg/m³, though one extreme sample's overpressure corresponds to a depth of  $\sim\!750\,$ m within the crust. The APAV lava is the only  $CO_2$ - $H_2O$  undersaturated sample in this study. Though it was collected at 178 bars of water pressure, its

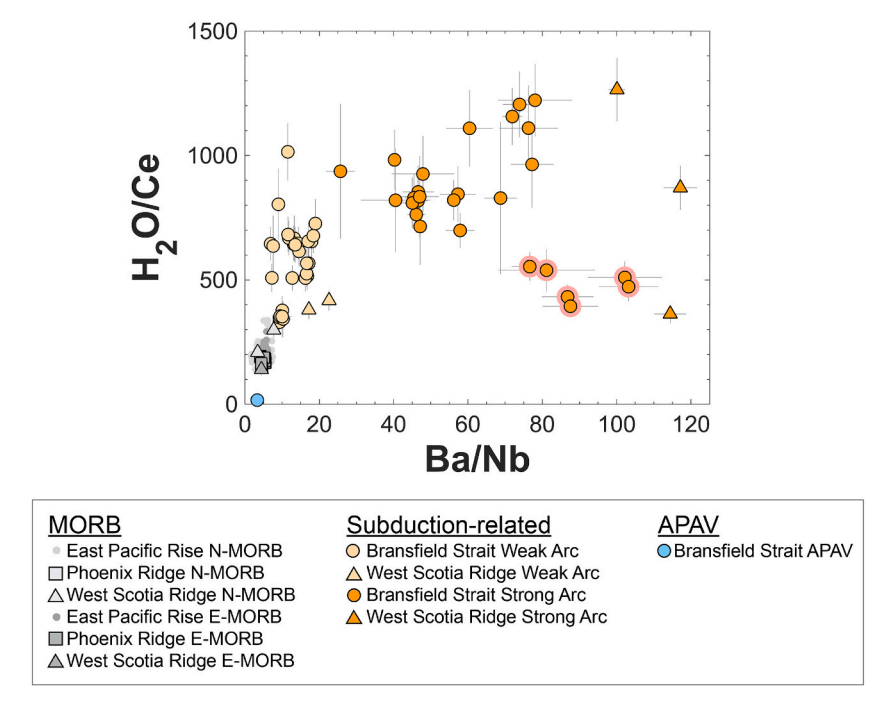


Fig. 8.  $H_2O/Ce$  vs Ba/Nb for the samples in this study and Pacific MORB, which has been filtered for assimilation of hydrothermally altered crust and brines (Shimizu et al., 2016). Errors for each ratio are propagated from each sample's  $2\sigma$  standard error for each element. In cases where the volatile calibration error was larger than the standard error, that was propagated instead.

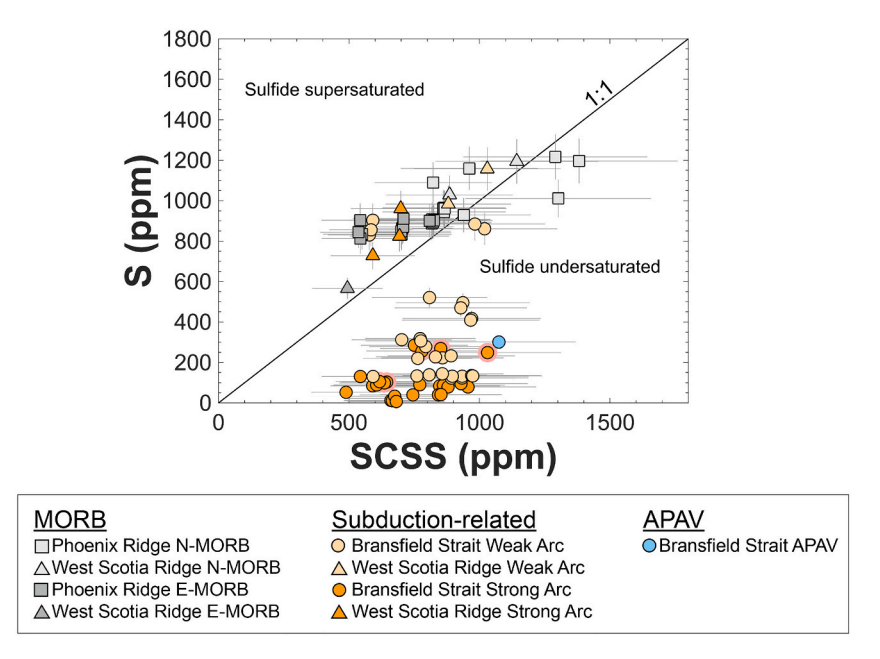


Fig. 9. Measured S content vs modeled sulfur content at sulfide saturation (SCSS), calculated using the model of Smythe et al. (2017). Given the errors of the model, the differences between the ideal and non-ideal sulfide solution models presented by Smythe et al. (2017) are negligible for our samples, so we use the ideal case. Samples plotting below the 1:1 line are sulfide undersaturated, whereas samples that fall within error of the line reached sulfide saturation prior to eruption. Vertical errors are each sample's  $2\sigma$  standard error for S. In cases where the calibration error was larger than the standard error for S, that was used instead. Horizontal errors are provided by the model.

extremely low  $CO_2$ - $H_2O$  contents yield a  $P_{sat}$  of 0 bars, suggesting either that its source is extremely  $CO_2$ - $H_2O$  depleted (unlikely) or the lava significantly degassed and erupted at subaerial pressures and was subsequently transported to its collection depth.

The  $CO_2$ - $H_2O$  of most Phoenix and West Scotia Ridge MORB overlap with the range for published Pacific MORB glasses, reflecting degassing and melt equilibration with a  $CO_2$ -dominant vapor phase (Fig. 5a). The alkaline E-MORB samples ( $H_2O > 1.0$  wt%) have somewhat lower  $H_2O$ 

contents for a given Ce content than the Pacific E-MORB, and they have exceptionally low  $\rm H_2O/Ce$ , which may indicate they degassed slightly more  $\rm H_2O$  than the tholeitic E-MORB (Figs. 4a and 7a). Yet, their F contents, which should not degas substantially at submarine pressures, correlate strongly with  $\rm H_2O$  and fall within range of Pacific MORB, suggesting this degassing has only minimally affected their  $\rm H_2O$  contents (Edmonds et al., 2009; Fig. 5c).

Lavas from the Bransfield Strait have extremely low CO2 and span a

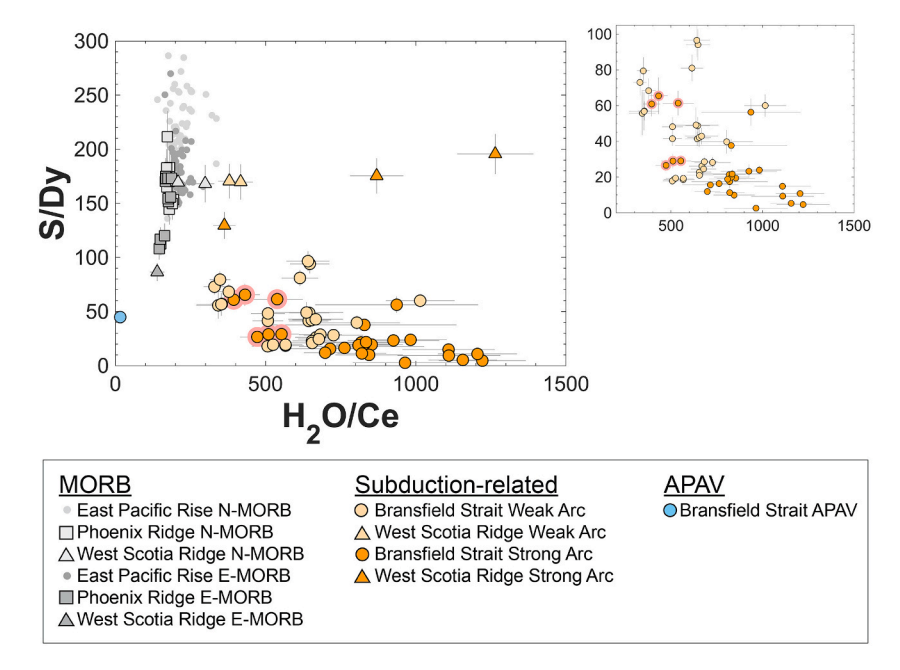


Fig. 10. S/Dy vs  $H_2O$ /Ce for the samples in this study and Pacific MORB, which has been filtered for assimilation of hydrothermally altered crust and brines (Shimizu et al., 2016). Inset shows negative correlation for Bransfield Strait arc-like lavas. Errors for each ratio are propagated from each sample's  $2\sigma$  standard error for each element. In cases where the volatile calibration error was larger than the standard error, that was propagated instead.

wide range of  $\rm H_2O$  contents, suggesting that they have significantly degassed and equilibrated with an  $\rm H_2O$ -dominant vapor phase (Fig. 5a). Degassing of this  $\rm H_2O$ -rich vapor phase likely resulted in some  $\rm H_2O$  loss in these samples (e.g., Wallace, 2005; Plank et al., 2013). However, positive correlations between  $\rm H_2O$  and F contents (Fig. 5c), as well as between  $\rm H_2O$ /Ce and subduction signal (e.g., Th/La and Ba/Nb; Figs. 7a and 8, respectively) suggest that despite  $\rm H_2O$  degassing, the  $\rm H_2O$ /Ce ratios of the Bransfield Strait lavas still reflect compositional differences in their sources (i.e., extent of subduction influence).

# 5.1.3. Contamination with hydrothermally altered material

Assimilation of hydrothermally altered crust and seawater-derived brines will elevate the Cl contents of a lava, making Cl a useful tool to assess contamination in MORB (e.g., Michael and Cornell, 1998; Shimizu et al., 2016). It is more difficult to assess these effects in subduction-derived melts, which are fluxed with significant amounts of Cl. However, since we intend to compare the Cl contents between the MORB and arc-like samples, we use Cl/Nb instead of Cl/K or Cl/Ba, since slab-derived fluids will elevate arc-like lavas in Cl, K, and Ba.

The MORB samples in this study show no signs of assimilation of hydrothermally altered crust in their Cl/Nb ratios. Compared to our MORB data, the Pacific MORB glasses from Shimizu et al. (2016) extend to higher Cl for a given Nb and higher Cl/Nb at similar values of Th/La, indicating Cl addition through assimilation of hydrothermally altered crust or brines. In contrast, the MORB samples of this study form a tight, shallow positive correlation (Figs. 4c, 5b, and 7b). Prior work suggested that decreasing spreading rates at the Phoenix Ridge resulted in progressively lower degree melts sampling increasingly trace element and isotope enriched sources (Haase et al., 2011; Anderson et al., 2023). The steady increase in Cl/Nb in the MORB samples with increasing Th/La is consistent with this shift to lower extents of melting and greater source enrichment, rather than contamination. Our data suggest that Cl/Nb ratios of uncontaminated N-MORB and E-MORB are roughly <15 and 20, respectively. The Pacific MORB data from Shimizu et al. (2016) are filtered on this basis in all figures except Figs. 4, 5, and 7b, where we are not considering differences in the volatile contents of their sources. For the arc-like lavas, high Cl/Nb ratios correlate with stronger subduction signals. The positive correlation between Cl/Nb and Th/La reflects a

high Cl input from slab fluids that corresponds well with increasing sediment flux (as indicated by Th/La). This increase in Cl/Nb could be controlled by assimilation of hydrothermally altered crust. At a given range in Th/La, many of the arc-like lavas show slight variations in Cl/Nb, which could be caused by some assimilation of hydrothermally altered crust or brine. However, these lavas display no clear changes in trace element or isotope ratios with decreasing MgO, suggesting assimilation is not the main control on their compositions.

# 5.1.4. Sulfide saturation and sulfur degassing

We calculated the sulfur content at sulfide saturation (SCSS) using the model of Smythe et al. (2017), which we then compared to the measured S concentrations of the lavas (Fig. 9). The SCSS of a melt depends heavily on pressure, temperature, melt composition, and fO2 (Smythe et al., 2017., Nash et al., 2019; O'Neill, 2021). We broadly assume MORB melt near the conditions of the favalite-magnetite-quartz (FMQ) oxygen buffer (Lee et al., 2005; O'Neill et al., 2018), but this may not be the case for the subduction-influenced lavas (Lee et al., 2005; Kelley and Cottrell, 2012; Plank and Forsyth, 2016). For this reason, we estimated the fO2 of the subduction-influenced lavas using the partitioning of V between olivine and melt after Canil (2002). The data collected for this model are presented in Supplementary Table S3. The  $fO_2$  values were then converted to proportions of Fe<sup>3+</sup> relative to total Fe (Fe<sup>3+</sup>/Fe<sub>T</sub>) using the model of Kress and Carmichael (1991). This conversion was done using pre-eruptive temperatures (using the thermometer of Wallace and Carmichael, 1992, calibrated using olivinediopside-silica multiple saturation experiments and correcting for the effect of H<sub>2</sub>O using Médard and Grove, 2008) at 0.1 GPa. Although we did not measure V in the MORB and APAV samples, we used the values presented in Kelley and Cottrell (2012) for the East Pacific Rise. Our values for  $Fe^{3+}/Fe_T$  at pre-eruptive conditions were  $\sim 0.17$  for MORB and APAV,  $\sim 0.20$  for arc-like West Scotia Ridge lavas, and  $\sim 0.25$  for Bransfield Strait lavas. We combined these fO2 estimates with the calculated pre-eruptive temperatures at 0.1 GPa to calculate SCSS for each sample.

The results of the model reveal that all samples from the Phoenix and West Scotia ridges are within error of sulfide saturation. As a result, any signal of source composition in the S contents of these lavas has likely

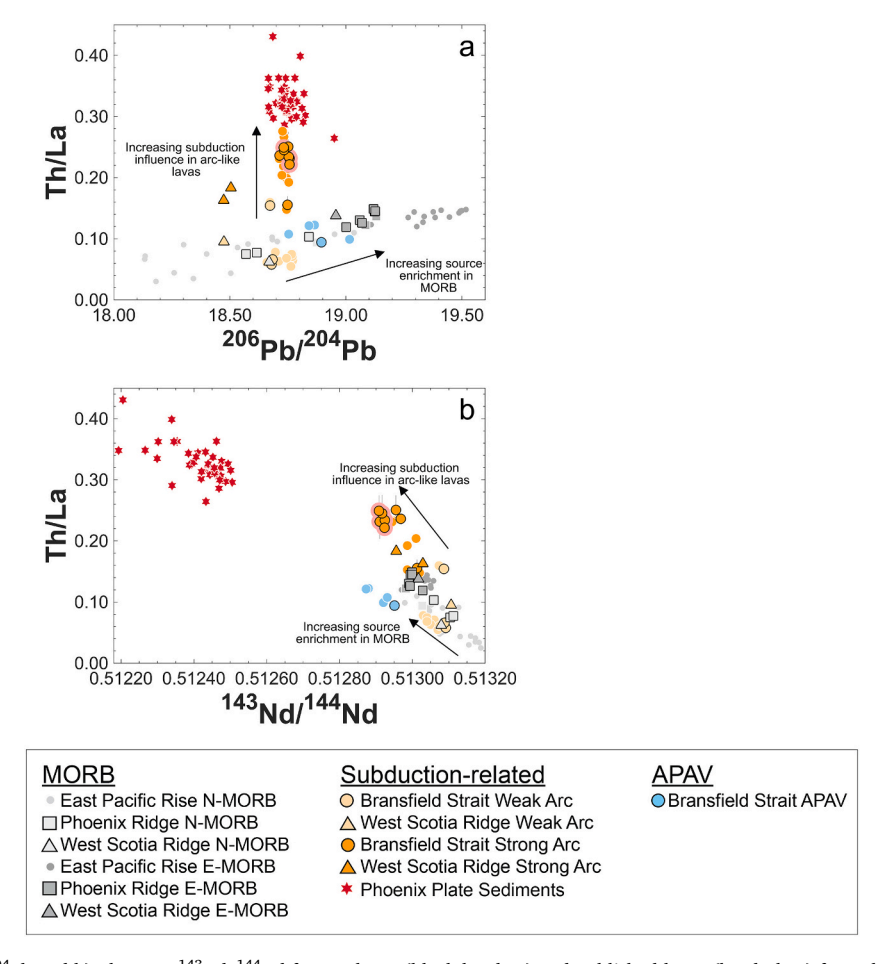


Fig. 11. a) Th/La vs  $^{206}$ Pb/ $^{204}$ Pb and b) Th/La vs  $^{143}$ Nd/ $^{144}$ Nd for our lavas (black borders) and published lavas (borderless) from the Phoenix Ridge (Haase et al., 2011), the Bransfield Strait (Keller et al., 1992; Keller and Fisk, 1992; Keller et al., 2002; Fretzdorff et al., 2004; Kraus et al., 2013), and the East Pacific Rise (filtered for assimilation of hydrothermally altered crust and brines; Shimizu et al., 2016). Red stars are data for sediments from the Phoenix Plate from Anderson et al. (2023). Vertical errors are propagated from each sample's  $2\sigma$  standard error for Th and La. Horizontal errors are smaller than symbols. (For interpretation of the references to color in this figure legend, the reader is referred to the web version of this article.)

been overprinted by sulfide saturation. Fig. 9 shows that the E-MORB require lower S to saturate than the N-MORB, on account of differences in melt chemistry, which may explain their lower absolute S contents (Figs. 4e, 5d, and 9). This also explains why the alkaline E-MORB (seen in Fig. 2) have particularly low S/Dy (Figs. 7e and 10). While their S contents are within range of other E-MORB, their Dy contents are elevated due to their lower extents of melting (Fig. 4e).

The  $fO_2$  of the arc-like samples seems to be the dominant variable controlling their S contents. Despite their strong subduction signals, arclike samples from the West Scotia Ridge are sulfide saturated and have lower fO<sub>2</sub> compared to the Bransfield Strait lavas, which have high fO<sub>2</sub> and are sulfide undersaturated. Despite their strong subduction signals, the West Scotia arc-like lavas have S/Dy ratios consistent with those of MORB, whereas the S/Dy ratios of the Bransfield Strait lavas roughly correlate negatively with subduction signal (Fig. 7e). This negative correlation suggests either the slab flux producing the subduction signal has low S/Dy or the melts have lost S during degassing. However, the S contents of arc magma sources are expected to be higher than those of the MORB mantle; therefore, S loss through degassing is a more viable explanation (De Hoog et al., 2001; Wallace, 2005; Taracsák et al., 2023). This S loss was likely spurred by high H<sub>2</sub>O contents and higher fO<sub>2</sub> (e.g., Liu et al., 2007; Wallace and Edmonds, 2011; Hughes et al., 2023; Ding et al., 2023). The negative correlation between S/Dy and H<sub>2</sub>O/Ce for the Bransfield Strait lavas in Fig. 10 supports this hypothesis. The effect of fO<sub>2</sub> on sulfide saturation and sulfur degassing in the West Scotia arc-like lavas can also be seen in Fig. 10, since the melts have similar values of S/Dy to those of MORB despite wide ranges in  $H_2O/Ce$  and strong subduction signals. The results of the SCSS model suggest that any signal of source variation in the S contents of the lavas has been overprinted by either sulfide saturation or degassing, so we will not consider S source contents any further.

# 5.2. Source variations in volatile contents

Having assessed the effects of secondary processes on the geochemistry of the lavas, we can assess variations in the volatile contents of their mantle sources. The  $\rm H_2O$ ,  $\rm CO_2$ , and S of the lavas have likely degassed to some extent and have, for the latter, additionally been affected by sulfide saturation. However, as indicated before,  $\rm H_2O$  degassing did not completely erase the initial  $\rm H_2O/Ce$  source signals of the lavas, and thus,  $\rm H_2O/Ce$  may still be informative of source composition. Only the APAV sample degassed so extensively that its  $\rm H_2O/Ce$  bears no source signal. Furthermore, secondary processes have not affected the Cl and F contents of the lavas, even for the extremely degassed APAV lava (Figs. 4, 5, and 7).

Fig. 11 demonstrates the strong relationship between Th/La and source composition. In the following discussion, we use Th/La as a proxy for source composition, which allows us to consider the source volatile contents of samples that do not have isotope data. Increasing Th/La in the MORB samples corresponds to greater isotopic source enrichment, whereas increasing Th/La in the arc-like lavas reflects greater subduction influence.

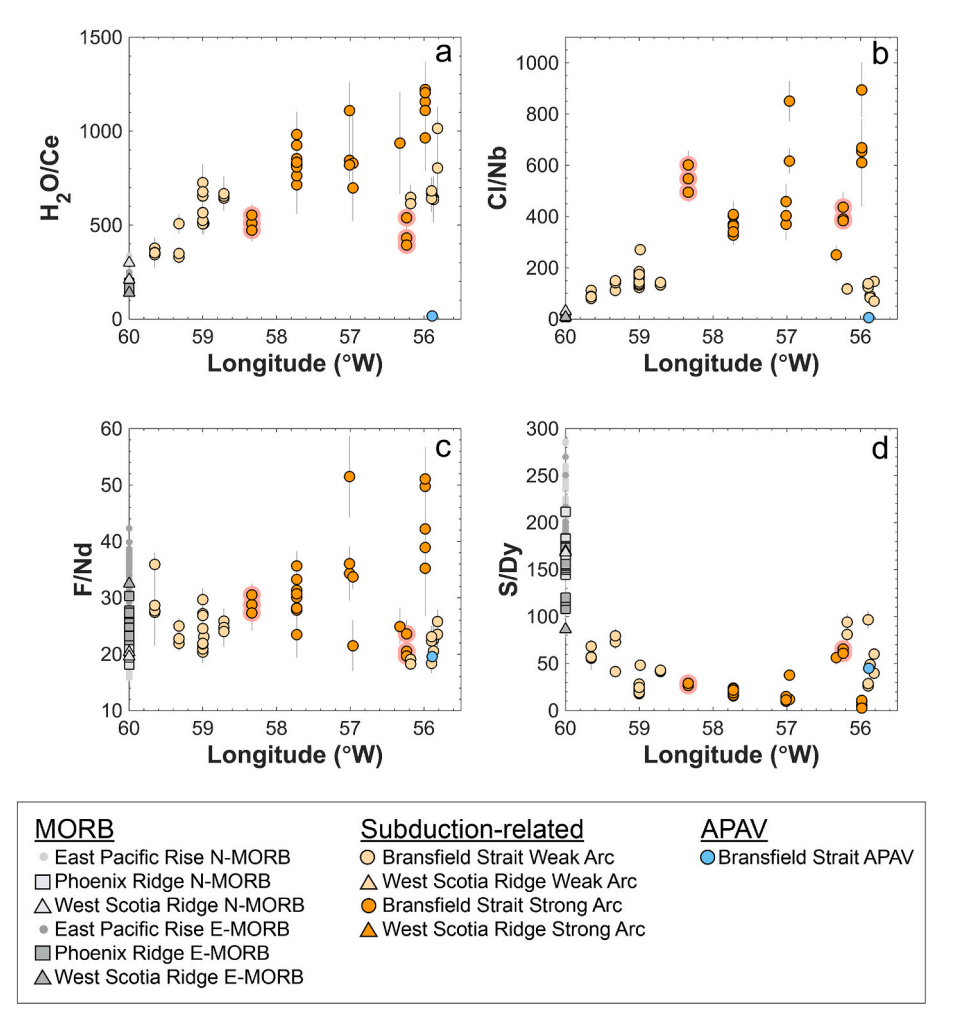


Fig. 12. Variations in a)  $H_2O/Ce$ , b) Cl/Nb, c) F/Nd, and d) S/Dy vs longitude for Bransfield Strait lavas. Data for Phoenix and West Scotia Ridge MORB are plotted on the vertical axis for reference, along with Pacific MORB data from Shimizu et al. (2016), which were filtered for assimilation of hydrothermally altered crust and brines. Vertical errors are propagated from each sample's  $2\sigma$  standard error for each element. In cases where the volatile calibration error was larger than the standard error, that was propagated instead.

# 5.2.1. Source variations in volatile contents of Phoenix and West Scotia Ridge MORB

Differences in volatile/refractory incompatible trace element ratios correspond well with source variations for the MORB samples (Fig. 7). The most trace element and isotope enriched MORB have the lowest  $\rm H_2O/Ce$  and  $\rm CO_2/Ba$  and the highest Cl/Nb and F/Nd. The lower  $\rm CO_2/Ba$ ratios in the E-MORB are jointly controlled by higher Ba concentrations and CO<sub>2</sub> degassing at similar pressures to the N-MORB samples (Fig. 6). The MORB samples follow a shallow negative correlation in H<sub>2</sub>O/Ce with increasing Th/La and appear to define mixtures of melts from a depleted MORB mantle (D-DMM) and a low-H2O/Ce enriched MORB mantle (E-DMM) (Fig. 7a). This was similarly observed in East Pacific Rise MORB by Shimizu et al. (2016), with many lavas varying little in H<sub>2</sub>O/Ce across broad ranges in Th/La. There are two possibilities to explain the low-H<sub>2</sub>O/Ce in E-MORB: They either melted from E-DMM with intrinsically low H<sub>2</sub>O/Ce (e.g., Dixon et al., 2002), or they melted from E-DMM with high initial H<sub>2</sub>O/Ce that subsequently experienced solid state H<sub>2</sub>O diffusive loss to the surrounding depleted mantle as proposed by Shimizu et al. (2016). Either way, Phoenix and West Scotia Ridge E-MORB seem to represent melting from an H<sub>2</sub>O/Ce-depleted E-DMM, resulting in the shallow trend observed in Fig. 7a.

Despite this  $H_2O/Ce$  depletion, our estimate for the  $H_2O$  concentration of Phoenix Ridge E-DMM is still slightly higher than that of DMM. For the most depleted N-MORB (average  $H_2O/Ce=187\pm15~2\sigma$  SD), we assume a DMM Ce concentration of 0.55 from Workman and Hart

(2005), which yields a DMM  $H_2O$  concentration of  $103\pm8$  ppm. Because the alkaline E-MORB samples may have degassed some  $H_2O$ , we only consider tholeiltic E-MORB (average  $H_2O/Ce=175\pm14~2\sigma$  SD) in our E-DMM estimate. We assume an E-DMM Ce concentration of 0.726 from Workman and Hart (2005), resulting in an E-DMM  $H_2O$  concentration of  $127\pm10$  ppm.

Furthermore, Cl/Nb and F/Nd correlate positively with source enrichment, and the MORB data from this study overlap with the Pacific MORB lavas from Shimizu et al. (2016). The slight offset in our data to slightly lower H<sub>2</sub>O/Ce, Cl/Nb, and F/Nd at a given Th/La suggest our samples define a lower bound for Pacific MORB (Fig. 7). The data indicate that for the Phoenix and West Scotia ridges, the E-MORB source is more enriched in H<sub>2</sub>O, Cl, and F than the N-MORB source, in agreement with what Shimizu et al. (2016) found for East Pacific Rise MORB. These findings support that the most enriched MORB, generated as spreading rates at the Phoenix Ridge decreased, were preferentially formed due to higher volatile contents and greater fertility of the E-MORB source (e.g., Choi et al., 2008; Haase et al., 2011).

# 5.2.2. Source variations in Bransfield Strait volatile contents

Bransfield Strait lavas show variations in volatile/refractory incompatible trace element ratios that correspond well with varying amounts of subduction input to their mantle sources. Positive correlations in  $\rm H_2O/Ce$ , Cl/Nb, and F/Nd vs Th/La support that increasing slab flux produces greater volatile enrichment (Fig. 7).

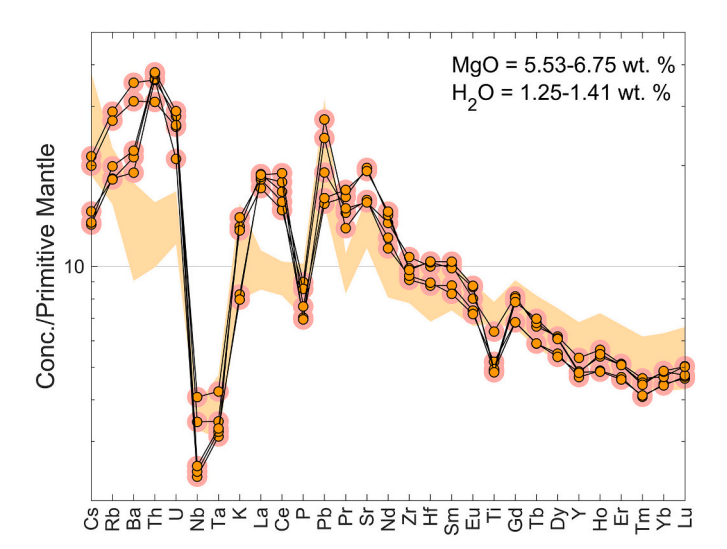


Fig. 13. Primitive mantle normalized trace element diagram of Bransfield Strait Strong Arc lavas with distinct incompatible trace element compositions. Orange background field represents the range of all other Bransfield Strait Strong Arc lavas at comparable MgO and  $\rm H_2O$  contents. Primitive mantle composition is from McDonough and Sun (1995). See Section 5.2.2 for details and discussion.

Furthermore, previous work has shown that Bransfield Strait lavas follow a gradual along-axis increase in subduction signal from SW to NE beginning at about 59°W until reaching about 56°W, where the signal sharply decreases (Fretzdorff et al., 2004; Anderson et al., 2023). Our volatile data reveal that this spatial compositional trend is also present in volatile/refractory incompatible trace element ratios (Fig. 12). Lavas with the highest H<sub>2</sub>O/Ce, Cl/Nb, and F/Nd are roughly found near the central-NE region of the back-arc, where the mantle wedge is expected to carry the strongest signs of subduction influence (Anderson et al., 2023). This makes sense because greater subduction influence should raise the volatile contents of the mantle, spurring high extents of melting and lowering the concentrations of similarly incompatible refractory elements. Indeed, Anderson et al. (2023) found that Bransfield Strait lavas bearing the strongest subduction signals melted to the greatest extents, an unsurprising effect of increased subduction influence. Interestingly, S/Dy forms the reverse trend, with the highest values occurring near the ends of the strait in the least subduction-modified lavas (Fig. 12d). This again is likely a function of the effect of fO2 (increasing with increased slab flux) and H2O degassing, which vary along the length of the of the Bransfield Strait —the areas where S/Dy is lowest correspond to the areas where H<sub>2</sub>O/Ce is highest (Figs. 10 and

The observed spatial geochemical trend along the Bransfield Strait is likely tied to the area's complex mantle dynamics. The Phoenix Ridge upper mantle has likely passed into the mantle wedge via toroidal flow around the edges of the Phoenix slab as the subduction angle has steepened through time, diluting the effects of subduction processes at the ends of the strait and forcing the most subduction-modified portions of the mantle wedge to the center (Anderson et al., 2023). This is why lavas that occur at the ends of the strait, areas that are in more direct contact with fresh inflowing sub-slab MORB mantle, have the weakest subduction signals and lowest volatile/refractory incompatible trace element ratios (Fig. 12). Our findings suggest that inflowing sub-slab asthenosphere into the mantle wedge may strongly influence spatial and compositional variations in back-arc basalts, especially in subduction zones with slab windows and tears.

A subset of Strong Arc lavas from the Bransfield Strait back-arc range to low  $H_2O/Ce$  and F/Nd and high S/Dy at high Th/La, deviating from the trends defined by other Bransfield Strait samples (Fig. 7, highlighted in pink). However, their range in volatile contents overlaps with that of

other Strong Arc lavas at comparable MgO contents and Th/La ratios (Figs. 4-5). Thus, their distinct H<sub>2</sub>O/Ce, F/Nd, and S/Dy ratios must, in part, be affected by their elevated Ce and Nd and lower Dy concentrations. This can be seen clearly when comparing their primitive mantlenormalized incompatible trace element patterns to those of other Strong Arc lavas at similar MgO and H2O contents (Fig. 13). Their relative depletions in Nb, Ta, Ti, and mid to heavy rare earth elements (REE) suggest that their mantle source was depleted in incompatible refractory trace elements before being affected by subduction processes (Fig. 13). In spite of this, these lavas have some of the most enriched isotope compositions in the Bransfield Strait, suggesting that recent melting of an isotopically enriched source produced this trace element depletion (Fig. 14). Their isotope compositions also suggest a connection to the enriched APAV lavas ubiquitously present throughout the Antarctic Peninsula (Fig. 14; e.g., Hole, 1990; Košler et al., 2009). We speculate that residual mantle from recent APAV melt generation beneath the Prince Gustav Rift region behind the Bransfield Strait has been dragged beneath the Bransfield Strait via corner flow and fluxed with subducted sediments and fluids, producing low degree melts (≤ 3% melting) with elevated incompatible trace element concentrations (e.g., Ce and Nd) and steep REE slopes (which may also indicate the presence of residual garnet in their source). Using the simple model presented in Supplementary Fig. S1, we show that this process could explain the compositions of these Strong Arc lavas from the Bransfield Strait. Although by no means is this the only possible explanation for their origins, this is a reasonable model to explain their trace element, volatile element, and radiogenic isotope compositions.

With only one sample, we cannot infer much about the volatile composition of the APAV source. However, despite the significant loss of  $\rm H_2O$ ,  $\rm CO_2$ , and S to degassing, the APAV lava appears to have retained its Cl and F. It is at least clear that the Cl/Nb and F/Nd of this single sample are very close to those of MORB, suggesting its source may at least have similar Cl/Nb and F/Nd to DMM (Fig. 7).

# 5.2.3. The origins of West Scotia Ridge arc-like lavas

The presence of arc-like lavas from the W7 segment of the West Scotia Ridge is rather surprising and not well understood. These lavas have subduction signals in their primitive mantle-normalized incompatible trace element patterns (Fig. 3), and our new data reveal that they also deviate from MORB in isotope space, extending towards a subduction-like radiogenic Pb-Sr-Hf and unradiogenic Nd endmember similar to the South Sandwich Arc (Fig. 14). Additionally, their elevated volatile/refractory incompatible trace element ratios correlate with subduction signal and further support they melted from a mantle source affected by subduction processes (Fig. 7).

Published <sup>40</sup>Ar-<sup>39</sup>Ar ages of 137–93 Ma suggest that these lavas are much older than the West Scotia Ridge itself, which only began spreading ~30 Ma at the earliest (Maldonado et al., 2014; Riley et al., 2019). To reconcile the unique geochemistry and ages of these lavas, previous workers suggested the W7 segment crust was part of a downfaulted block of the Cretaceous Tierra del Fuegian Andes, parts of which were dragged >1200 km eastwards along the North Scotia Ridge fault during the opening of the Scotia Plate (Riley et al., 2019; Fig. 1a). However, our volatile data are inconsistent with this interpretation. Calculated Psat for each sample fall within error of their Pcoll, suggesting that since erupting, these lavas have not experienced any significant changes in bathymetry (Fig. 6). This is at odds with a supposed Tierra del Fuegian Andes origin, since the lavas would need to have survived substantial changes in depth over a  $\sim 100$  Myr period of significant tectonic reconfiguration (e.g., Dalziel et al., 2013; Eagles and Jokat, 2014; van de Lagemaat et al., 2021). Furthermore, in discussing their geochronology, Riley et al. (2019) acknowledged there is evidence of <sup>39</sup>Ar recoil, leaving open the possibility that the ages themselves could be artificially older.

We propose that these W7 lavas are recent melts (~6 Ma based on their proximity to the ridge axis) that sampled a subduction-modified

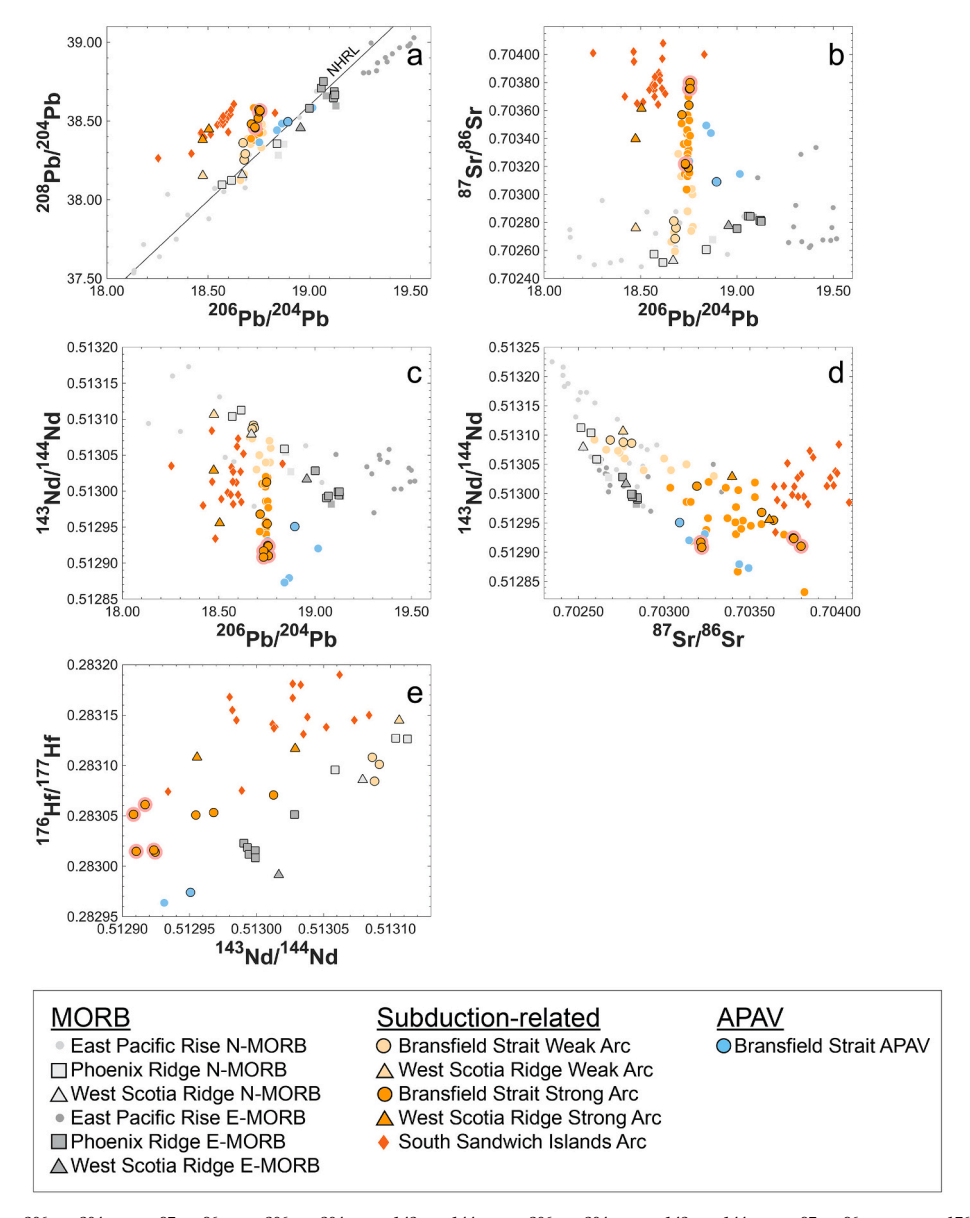


Fig. 14. a) <sup>208</sup>Pb/<sup>204</sup>Pb vs <sup>206</sup>Pb/<sup>204</sup>Pb, b) <sup>87</sup>Sr/<sup>86</sup>Sr vs <sup>206</sup>Pb/<sup>204</sup>Pb, c)<sup>143</sup>Nd/<sup>144</sup>Nd vs <sup>206</sup>Pb/<sup>204</sup>Pb, d) <sup>143</sup>Nd/<sup>144</sup>Nd vs <sup>87</sup>Sr/<sup>86</sup>Sr, and e) <sup>176</sup>Hf/<sup>177</sup>Hf vs <sup>143</sup>Nd/<sup>144</sup>Nd for lavas from the Phoenix Ridge (Haase et al., 2011; Anderson et al., 2023), West Scotia Ridge (Anderson et al., 2023; This study), Bransfield Strait (Keller et al., 1992; Keller and Fisk, 1992; Keller et al., 2002; Fretzdorff et al., 2004; Anderson et al., 2023; This study), East Pacific Rise (filtered for assimilation of hydrothermally altered crust and brines; Shimizu et al., 2016), and South Sandwich Arc (Leat et al., 2004; Barry et al., 2006). Symbols with black borders represent samples in this study. Errors for our data are smaller than the symbols.

mantle left behind by an earlier subduction zone —likely an ancient predecessor of the modern South Sandwich subduction zone (Fig. 1a). Tectonic reconstructions of the Scotia Sea region are greatly debated, but one thing most have in common is that roughly 20-30 Ma a subduction zone existed in the area where the W7 segment currently lies (Eagles and Jokat, 2014; van de Lagemaat et al., 2021). Based on the geochemistry of lavas at the W7 segment, it appears that some subduction-modified mantle was left behind as the Scotia Plate continued rapidly expanding eastwards. Whether this mantle remained as ambient asthenosphere or as metasomatized lithosphere is unclear. Regardless, there are undeniable geochemical similarities between W7 lavas and arc lavas from the South Sandwich subduction zone. In isotope space, the W7 samples bearing the strongest subduction signals coincide perfectly with lavas from the South Sandwich Arc, whereas the W7 lavas with the weakest subduction signals back-project towards N-MORB compositions (Fig. 14). This suggests that some portions of the West Scotia Ridge overlie mantle that was modified by subduction processes

during the eastward migration of the South Sandwich Arc and the opening of the Scotia Plate. Our findings underscore the enduring impact subduction processes have on the upper mantle, even in regions that today are hundreds of kilometers from the nearest subduction zone. This calls into question our understanding of the lifetime and distribution of subduction-derived material persisting in the upper mantle across the Earth, something that has begun to be recognized at other ridges as well (Yang et al., 2021).

As previously discussed, these W7 lavas have higher S/Dy ratios (within the range of MORB) than the arc-like lavas from the Bransfield Strait, and they are the only sulfide saturated Strong Arc samples (Fig. 7e and 9). This suggests that these lavas did not lose S to degassing like the other Bransfield Strait lavas on account of their somewhat lower  $fO_2$  (see Section 5.1.4 and Supplementary Table S3 for details), despite their high  $H_2O$  contents (Figs. 5d and 10) and strong evidence of subduction influence in their trace element and isotope compositions (Figs. 3 and 14, respectively). Even though some subduction-modified mantle underlies

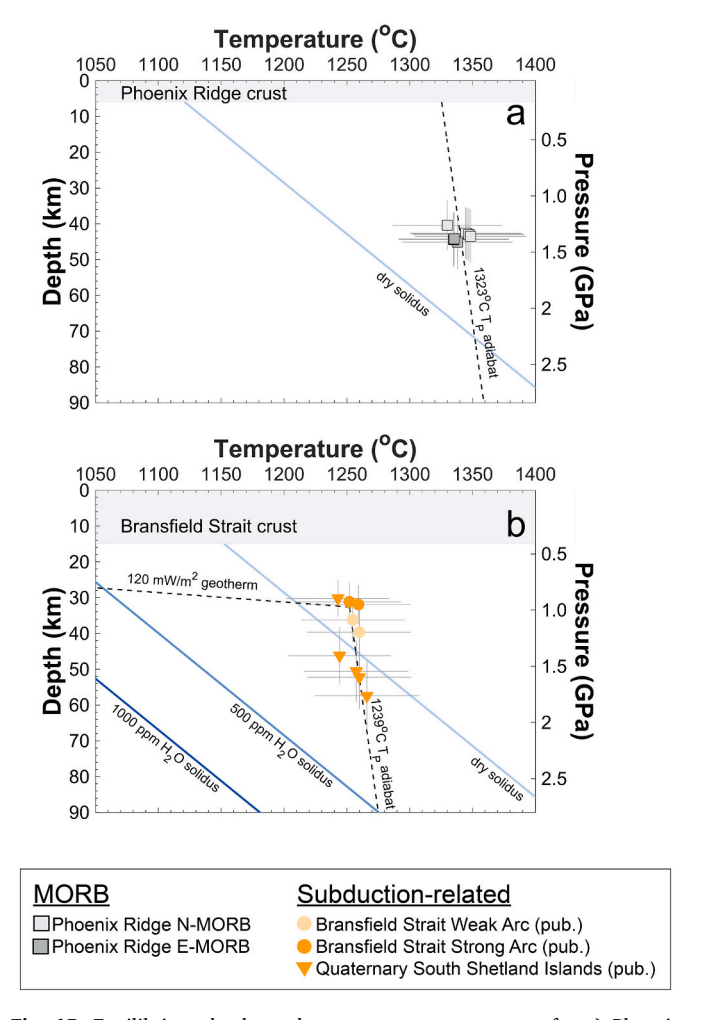
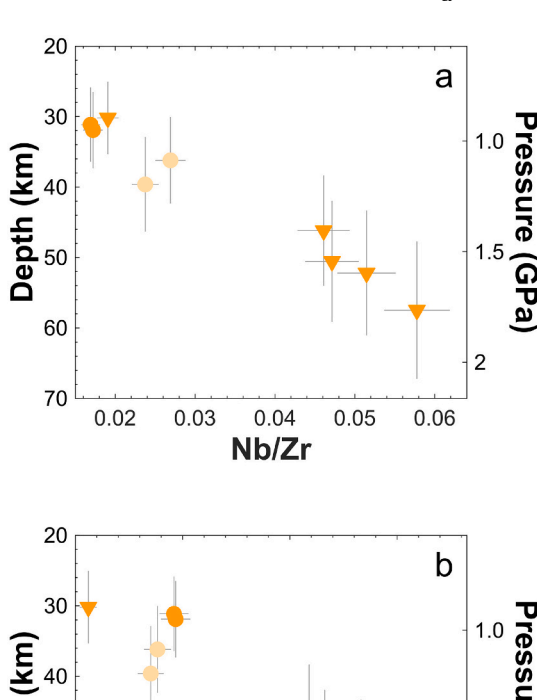


Fig. 15. Equilibrium depths and pressures vs temperatures for a) Phoenix Ridge lavas (this study; marked with black borders) and b) Bransfield Strait (Fretzdorff et al., 2004) and Quaternary South Shetland Island (Haase et al., 2012) lavas, modeled using Plank and Forsyth (2016). Depths were calculated assuming 6 km and 15 km crust, respectively, assuming a crustal density of 2800 kg/m<sup>3</sup> and a mantle density of 3250 kg/m<sup>3</sup>. Also plotted are the dry peridotite solidus from Plank and Forsyth (2016), and 500 and 1000 ppm H<sub>2</sub>O solidi after Katz et al. (2003). Additionally, 1323 °C and 1239 °C adiabats in a) and b), respectively, were calculated assuming an adiabatic gradient of 0.4 °C/ km. A simple, steady-state conductive geotherm was calculated in b) using a 120 mW/m<sup>2</sup> surface heatflow (Lawver et al., 1995; Kaminuma and Nagao, 1996; Schreider et al., 2015), 15 km crust (Christeson et al., 2003), a lithospheric mantle heat production of  $0.03 \mu W/m^3$  (Rudnick et al., 1998), and a crustal heat production of 0.4 µW/m<sup>3</sup> (Rudnick et al., 1998). Error bars were calculated by propagating the uncertainties of equilibrium mantle Fo ( $\pm$  1), melt Fe<sup>3+</sup>/Fe<sub>T</sub> ( $\pm$  0.03), and melt H<sub>2</sub>O concentration ( $\pm$  5% relative) through the model. See Section 5.3 of the text for details and discussion.

the W7 segment, the melts do not seem to be especially oxidized, which is unusual for subduction modified melts (e.g., Kelley and Cottrell, 2009; Cottrell et al., 2021). We cannot rule out the possibility that the subduction modified source component of the W7 lavas is part of the oceanic lithospheric mantle.

# 5.3. Equilibrium pressure and temperature estimates

We estimated the pressure (P) and temperature (T) conditions of melts in equilibrium with the solid mantle using the  $H_2O$  contents, major element compositions, and  $Fe^{3+}/Fe_T$  ratios at mantle conditions, which we determined iteratively using measured V olivine-melt partition coefficients for each compositional group (see Section 5.1.4 and



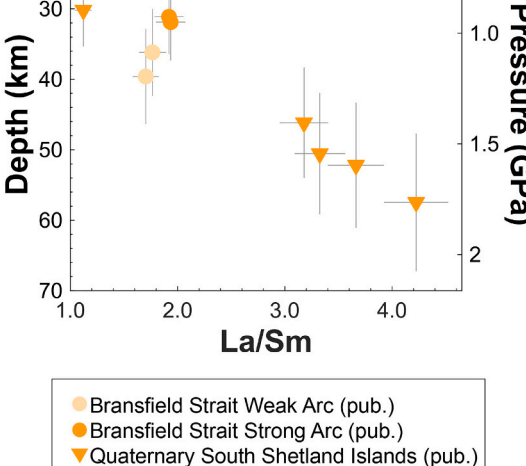


**Fig. 16.** Modeled equilibrium depths and pressures vs a) Nb/Zr and b) La/Sm for Bransfield Strait (Fretzdorff et al., 2004) and Quaternary South Shetland Island (Haase et al., 2012) lavas. Vertical errors and depth calculations are the same as those in Fig. 15. Horizontal errors are propagated from uncertainties reported by Fretzdorff et al. (2004) and Haase et al. (2012).

Supplementary Table S3 for details). At each iterative step, samples were fractionation-corrected to be in equilibrium with Fo90 by adding equilibrium olivine in 0.1% increments, and then these corrected compositions were used to estimate mantle pressures and temperatures using the model of Plank and Forsyth (2016). Values for Fe³+/Fe $_{\rm T}$  were then recalculated following the model of Kress and Carmichael (1991), and these steps were repeated until the values converged. Mantle Fe³+/Fe $_{\rm T}$  estimates for the Phoenix Ridge MORB and Bransfield Strait arc-like lavas were  $\sim 0.12$  and  $\sim 0.19$ , respectively. These estimates are reasonable given the range of published values for MORB and back-arc lavas and the uncertainties of the calculation. Though the Plank and Forsyth (2016) model is calibrated for melts in equilibrium with only olivine and orthopyroxene, we applied it here as a rough estimate of equilibrium P-T conditions for Phoenix Ridge and Bransfield Strait lavas.

The model requires fractionation-corrected primitive melt compositions, so we only used samples with MgO  $\sim$ 8.0 wt% or greater, where we could be confident that they have only crystallized olivine. In the Phoenix Ridge, this is not a problem, since many of our glass samples are sufficiently primitive. However, in the Bransfield Strait, only a few published samples from Fretzdorff et al. (2004) are primitive enough to apply the model. For these primitive samples, we estimated their H<sub>2</sub>O

contents using representative  $H_2O/Ce$  values from our data and measured Ce contents from Fretzdorff et al. (2004). For Weak Arc lavas, we used a  $H_2O/Ce$  value of 668, and for Strong Arc lavas, we used a value of 1157 (Fig. 7a). These values come from samples in our study with similar incompatible trace element patterns to those of the selected Fretzdorff et al. (2004) high MgO lavas. Additionally, we applied the model to a set of primitive Quaternary South Shetland Island volcanic front samples from Haase et al. (2012) as analogs for Bransfield Strait Strong Arc lavas. Anderson et al. (2023) found that these lavas have very similar trace element and isotope compositions to Bransfield Strait Strong Arc lavas, distinct from older (> 30 Ma) South Shetland Island lavas. We estimated the  $H_2O$  contents of these Quaternary South Shetland lavas using the same representative Strong Arc  $H_2O/Ce$  value of 1157. More details on these selections are provided in Supplementary Table S4.

Results for Phoenix Ridge MORB are all within error of each other, recording equilibrium conditions of  $\sim 1.35$  GPa ( $\sim 43$  km depth) and  $\sim 1340~{\rm C}$  (Fig. 15a). These conditions may reflect stalling at a boundary, possibly the lithosphere-asthenosphere boundary, since polybaric melt segregation along an adiabat would form a steep P-T trend (see reference adiabats in Fig. 15). Assuming a mantle adiabatic gradient of 0.4 °C/km (after Plank and Forsyth, 2016), the MORB samples would fall along an adiabat with a potential temperature of  $\sim 1323 \pm 43~{\rm ^{\circ}C}$ , which is reasonable for MORB (Klein and Langmuir, 1987; Falloon et al., 2007; Dalton et al., 2014; Fig. 15a).

Despite broad uncertainties in the model, the calculated equilibrium P-T of arc-like samples from the Bransfield Strait and Quaternary South Shetland Islands show resolvable variations in P at similar ranges in T (Fig. 15b). Given their steep trend in P-T, these melts may represent discrete partial melts that formed along an adiabat. If this is the case, the most incompatible trace element-depleted lavas should record the shallowest pressures, reflecting increasing extents of melting upon ascent. In fact, we observe strong correlations between modeled equilibrium P and incompatible trace element enrichment (Fig. 16). The results also show that the mantle began melting below the dry peridotite solidus, which is unsurprising because back-arc mantle should be elevated in H<sub>2</sub>O. Assuming the results reflect final equilibration in the asthenosphere, the shallowest results would put the maximum depth of the lithosphere-asthenosphere boundary beneath the strait at  $\sim 30$  km, broadly consistent with seismic data (Wiens et al., 2023). Again, assuming the same mantle adiabatic gradient of 0.4 °C/km, the arc-like samples fall along an adiabat with a potential temperature of  $\sim 1239 \pm$ 41 °C (Fig. 15b). This is somewhat low compared to the back-arc estimates of Wiens et al. (2006) but not unreasonable for Bransfield Strait melts, which have higher H2O contents than the melts they use —the imposed H<sub>2</sub>O/Ce values we use yield average H<sub>2</sub>O contents of ~ 2 wt% for our selected Bransfield Strait samples, compared to values ≤1 wt% in Wiens et al. (2006).

# 6. Conclusions

We have reported the first volatile element concentrations in the northern Antarctic Peninsula, revealing several important spatial and compositional relationships that hold broad implications for subduction worldwide.

Our findings support that as spreading rates slowed at the Phoenix ridge, preferential melting of less abundant, more fertile and volatile-rich *E*-DMM produced increasingly isotope and trace element enriched melt compositions.

In the Bransfield Strait, volatile enrichment corresponds strongly with increased subduction signal and increased degree of melting. These increases occur near the middle and NE portion of the strait, where the subduction-modified mantle is being forced by incoming sub-slab asthenosphere flowing toroidally around the slab's edges. Therefore, it is important to consider the potential influence sub-slab asthenosphere may have on the geochemistry of arc and back-arc lavas located near the

edges of subducting plates at other subduction zones, especially those with slab windows and tears that offer easy pathways into the mantle wedge. Furthermore, several Bransfield Strait samples have strong subduction signals but unusually low volatile/refractory incompatible trace element ratios. We suggest these samples reflect flux melting of residual enriched mantle, brought beneath the Bransfield Strait via corner flow following recent generation of alkaline lavas in the far eastern regions of the Antarctic Peninsula, highlighting the heterogeneous nature of the mantle wedge.

New data on arc-like lavas from the W7 segment of the West Scotia Ridge suggest they were collected in-situ and erupted perhaps as recently as 6 Ma. Their trace element and isotopic compositions suggest the W7 segment overlies subduction-modified mantle left behind within the past  $\sim 30$  Myr by the eastward-migrating South Sandwich Arc. The fact that this mantle remains beneath an area that is now hundreds of kilometers from the nearest subduction zone illustrates the enduring and widespread effects of subduction modification on the upper mantle.

Finally, modeled equilibrium P-T for Phoenix Ridge MORB suggest they accumulated at relatively uniform conditions, possibly at the lithosphere-asthenosphere boundary. In contrast, modeled P-T for lavas from the Bransfield Strait suggest they are discrete partial melts that formed along a mantle adiabat. Estimated mantle potential temperatures for both sets of lavas are consistent with ranges for mid-ocean ridges and subduction zones, respectively.

# **Declaration of Competing Interest**

The authors declare that they have no known competing financial interests or personal relationships that could have appeared to influence the work reported in this paper.

# Acknowledgements

We would like to thank Joe Boesenberg for his assistance with the electron microprobe analyses, Kayla Iacovino and Mark Ghiorso for their help accessing and navigating the VESIcal web-app, Karen Fischer for her help in calculating a geotherm, three anonymous reviewers for their helpful comments and suggestions, and Marco Fiorentini for his editorial handling. This study was supported by NSF OPP-ANT Earth Sciences 1643494 to AES.

# Appendix A. Supplementary data

Supplementary data to this article can be found online at https://doi. org/10.1016/j.chemgeo.2023.121839.

# References

- Anderson, D.W., Saal, A.E., Lee, J.I., Mallick, S., Riley, T.R., Keller, R.A., Haase, K.M., 2023. Tracing mantle components and the effect of subduction processes beneath the northern Antarctic Peninsula. Geochim. Cosmochim. Acta 343, 234–249.
- Baker, P.E., McReath, I., Harvey, M.R., Roobol, M.J., Davies, T.G., 1975. The geology of the South Shetland Islands: V. volcanic evolution of Deception Island. British Antarc. Surv. Sci. Rep. 78, 1–81.
- Barker, P.F., 1982. The Cenozoic subduction history of the Pacific margin of the Antarctic Peninsula: ridge crest-trench interactions. J. Geol. Soc. Lond. 139, 787–801.
- Barry, T.L., Pearce, J.A., Leat, P.T., Millar, I.L., le Roex, A.P., 2006. Hf isotope evidence for selective mobility of high-field-strength elements in a subduction setting: South Sandwich Islands. Earth Planet. Sci. Lett. 252, 223–244.
- Canil, D., 2002. Vanadium in peridotites, mantle redox and tectonic environments: Archean to present. Earth Planet. Sci. Lett. 195, 75–90.
- Choe, W.H., Lee, J.I., Lee, M.J., Hur, S.D., Jin, Y.K., 2005. New approach on the extinction of spreading at the Phoenix Ridge, Antarctica. J. Petrol. Soc. Korea 14, 73–81.
- Choi, S.H., Choe, W.H., Lee, J.I., 2008. Mantle heterogeneity beneath the Antarctic-Phoenix Ridge off Antarctic Peninsula. Island Arc 17, 172–182.
- Christeson, G.L., Barker, D.H.N., Austin, J.A., Dalziel, I.W.D., 2003. Deep crustal structure of Bransfield Strait: initiation of a back arc basin by rift reactivation and propagation. J. Geophys. Res. 108, 1–21.

- Cottrell, E., Birner, S.K., Brounce, M., Davis, F.A., Waters, L.E., Kelley, K.A., 2021.
  Oxygen fugacity across tectonic settings. In: Moretti, R., Neuville, D.R. (Eds.), AGU Geophysical Monograph Series Magma Redox Geochemistry, pp. 33–61.
- Dalton, C.A., Langmuir, C.H., Gale, A., 2014. Geophysical and geochemical evidence for deep temperature variations beneath mid-ocean ridges. Science 344, 80–83.
- Dalziel, I.W.D., Lawver, L.A., Norton, I.O., Gahagan, L.M., 2013. The Scotia arc: genesis, evolution, global significance. Annu. Rev. Earth Planet. Sci. 41, 767–793.
- Danyushevsky, L.V., Eggins, S.M., Falloon, T.J., Christie, D.M., 2000. H<sub>2</sub>O abundance in depleted to moderately enriched mid-ocean ridge magmas; part I: Incompatible behaviour, implications for mantle storage, and origin of regional variations. J. Petrol. 41, 1329–1364.
- De Hoog, J.C.M., Mason, P.R.D., Van Bergen, M.J., 2001. Sulfur and chalcophile elements in subduction zones: constraints from a laser ablation ICP-MS study of melt inclusions from Galunggung volcano, Indonesia. Geochim. Cosmochim. Acta 65, 3147–3164.
- Ding, S., Plank, T., Wallace, P.J., Rasmussen, D.J., 2023. Sulfur\_X: a model of sulfur degassing during magma ascent. Geochem. Geophys. Geosyst. 24, 1–30.
- Dixon, J.E., Stolper, E.M., 1995. An experimental study of water and carbon dioxide solubilities in mid-ocean ridge basaltic liquids. Part II: applications to degassing. J. Pet. 36, 1633–1646.
- Dixon, J., 1997. Degassing of alkalic basalts. American Mineralogist 82, 368–378.Dixon, J.E., Leist, L., Langmuir, C., Schilling, J.G., 2002. Recycled dehydrated lithosphere observed in plume-influenced mid-ocean-ridge basalt. Nature 420, 385–389
- Eagles, G., 2010. The age and origin of the central Scotia Sea. Geophys. J. Int. 183, 587–600.
- Eagles, G., Jokat, W., 2014. Tectonic reconstructions for paleobathymetry in Drake Passage. Tectonophysics 611, 28–50.
- Eagles, G., Livermore, R.A., Fairhead, J.D., Morris, P., 2005. Tectonic evolution of the west Scotia Sea. J. Geophys. Res. 110, 1–19
- Edmonds, M., Gerlach, T.M., Herd, R.A., 2009. Halogen degassing during ascent and eruption of water-poor basaltic magma. Chem. Geol. 263, 122–130.
- Falloon, T.J., Danyushevsky, L.V., Ariskin, A., Green, D.H., Ford, C.E., 2007. The application of olivine geothermometry to infer crystallization temperatures of parental liquids: implications for the temperature of MORB magmas. Chem. Geol. 241, 207-233.
- Fretzdorff, S., Worthington, T.J., Haase, K.M., Hékinian, R., Franz, L., Keller, R.A., Stoffers, P., 2004. Magmatism in the Bransfield Basin: rifting of the South Shetland Arc? J. Geophys. Res. 109, 1–19.
- Ghiorso, M.S., Gualda, G.A.R., 2015. An H<sub>2</sub>O-CO<sub>2</sub> mixed fluid saturation model compatible with rhvolite-MELTS. Contrib. Mineral, Petrol. 169, 1–30.
- Guenthner, W.R., Barbeau, D.L., Reiners, P.W., Thomson, S.N., 2010. Slab window migration and terrane accretion preserved by low-temperature thermochronology of a magmatic arc, northern Antarctic Peninsula. Geochem. Geophys. Geosyst. 11, 1–13.
- Haase, K.M., Beier, C., 2021. Chapter 3.2b Bransfield Strait and James Ross Island: petrology. Geol. Soc. Lond. Mem. 55, 1–17.
- Haase, K.M., Beier, C., Fretzdorff, S., Leat, P.T., Livermore, R.A., Barry, T.L., Pearce, J.A., Hauff, F., 2011. Magmatic evolution of a dying spreading axis: evidence for the interaction of tectonics and mantle heterogeneity from the fossil Phoenix Ridge, Drake Passage. Chem. Geol. 280, 115–125.
- Haase, K.M., Beier, C., Fretzdorff, S., Smellie, J.L., Garbe-Schönberg, D., 2012. Magmatic evolution of the South Shetland Islands, Antarctica, and implications for continental crust formation. Contrib. Mineral. Petrol. 163, 1103–1119.
- Hauri, E., Wang, J., Dixon, J.E., King, P.L., Mandeville, C., Newman, S., 2002. SIMS analysis of volatiles in silicate glasses 1. Calibration, matrix effects and comparisons with FTIR. Chem. Geol. 183, 99–114.
- Hole, M.J., 1990. Geochemical evolution of Pliocene-recent post-subduction alkalic basalts from Seal Nunataks, Antarctic Peninsula. J. Volcanol. Geotherm. Res. 40, 149–167
- Hole, M.J., 2021. Chapter 4.1b Antarctic Peninsula: petrology. Geol. Soc. Lond. Mem. 55, 1-17.
- Hole, M.J., Saunders, A.D., Rogers, G., Sykes, M.A., 1994. The relationship between alkaline magmatism, lithospheric extension, and slab window formation along continental destructive plate margins. Geol. Soc. Spec. Publ. 81, 265–285.
- Hughes, E.C., Saper, L., Liggins, P., O'Neill, H.S.C., Stolper, E.M., 2023. The sulfur solubility minimum and maximum in silicate melt. J. Geol. Soc. Lond. https://doi. org/10.1144/jgs2021-125.
- Iacovino, K., Matthews, S., Wieser, P.E., Moore, G.M., Bégué, F., 2021. VESIcal Part I: an open-source thermodynamic model engine for mixed volatile (H<sub>2</sub>O-CO<sub>2</sub>) solubility in silicate melts. Earth Space Sci. 8, 1–55.
- Johnson, M.C., Plank, T., 2000. Dehydration and melting experiments constrain the fate of subducted sediments. Geochem. Geophys. Geosyst. 1, 1–26.
- Jordan, T.A., Riley, T.R., Siddoway, C.S., 2020. The geological history and evolution of West Antarctica. Nat. Rev. Earth Env. 1, 117–133.
- Kaminuma, K., Nagao, T., 1996. Heat flow measurements in the Antarctic Peninsula region. Korean J. of Pol. Res. 7, 29–33.
- Katz, R.F., Spiegelman, M., Langmuir, C.H., 2003. A new parameterization of hydrous mantle melting. Geochem. Geophys. Geosyst. 4, 1–19.
- Keller, R.A., Fisk, M.R., 1992. Quaternary marginal basin volcanism in the Bransfield Strait as a modern analogue of southern Chilean ophiolites. Geol. Soc. Spec. Publ. 60, 155–169.
- Keller, R.A., Fisk, M.R., White, W.M., Birkenmajer, K., 1992. Isotopic and trace element constraints on mixing and melting models of marginal basin volcanism, Bransfield Strait, Antarctica. Earth Planet. Sci. Lett. 60, 155–169.

Keller, R.A., Fisk, M.R., Smellie, J.L., Strelin, J.A., Lawver, L.A., 2002. Geochemistry of back arc basin volcanism in Bransfield Strait, Antarctica: subducted contributions and along-axis variations. J. Geophys. Res. 107, 1–17.

- Kelley, K.A., Cottrell, E., 2009. Water and the oxidation state of subduction zone magmas. Science 325, 605–607.
- Kelley, K.A., Cottrell, E., 2012. The influence of magmatic differentiation on the oxidation state of Fe in a basaltic arc magma. Earth Planet. Sci. 329–330, 109–121.
- Klein, E.M., Langmuir, C.H., 1987. Global correlations of ocean ridge basalt chemistry with axial depth and crustal thickness. J. Geophys. Res. 92, 8089–8115.
- Košler, J., Magna, T., Mlčoch, B., Mixa, P., Nývlt, D., Holub, F.V., 2009. Combined Sr, Nd, Pb and Li isotope geochemistry of alkaline lavas from northern James Ross Island (Antarctic Peninsula) and implications for back-arc magma formation. Chem. Geol. 258, 207–218.
- Kraus, S., Kurbatov, A., Yates, M., 2013. Geoquímica de tefras de volcanes cuaternarios de la Península Antártica. Andean Geol. 40, 1–40.
- Kress, V.C., Carmichael, I.S.E., 1991. The compressibility of silicate liquids containing Fe2O3 and the effect of composition, temperature, oxygen fugacity and pressure on their redox states. Contrib. Mineral. Petrol. 108, 82–92.
- Lawver, L.A., Keller, R.A., Fisk, M.R., Strelin, J.A., 1995. Bransfield Strait, Antarctic Peninsula active extension behind a dead arc. In: Backarc Basins: Tec. Mag., pp. 315–342.
- Leat, P.T., Riley, T.R., 2021a. Chapter 3.1a Antarctic Peninsula and South Shetland Islands: volcanology. Geol. Soc. Lond. Mem. 55, 1–28.
- Leat, P.T., Riley, T.R., 2021b. Chapter 3.1b Antarctic Peninsula and South Shetland Islands: petrology. Geol. Soc. Lond. Mem. 55, 1–14.
- Leat, P.T., Pearce, J.A., Barker, P.F., Millar, I.L., Barry, T.L., Larter, R.D., 2004. Magma genesis and mantle flow at a subducting slab edge: the South Sandwich arc-basin system. Earth Planet. Sci. Lett. 227, 17–35.
- Lee, J.I., Park, B.K., Jwa, Y.J., Yoon, H.I., Yoo, K.C., Kim, Y., 2005. Geochemical characteristics and the provenance of sediments in the Bransfield Strait, West Antarctica. Mar. Geol. 219, 81–98.
- Liu, Y., Samaha, N.-T., Baker, D.R., 2007. Geochem. Cosmochim. Acta 71, 1783–1799.
  Livermore, R., Balanyá, J.C., Maldonado, A., Martínez, J.M., Rodríguez-Fernández, J.,
  Sanz de Galdeano, C., Galindo, Zaldívar J., Jabaloy, A., Barnolas, A., Somoza, L.,
  Hernández-Molina, J., Suriñach, E., Viseras, C., 2000. Autopsy on a dead spreading center: the Phoenix Ridge, Drake Passage, Antarctica. Geology 28, 607–610.
- MacDonald, G.A., Katsura, T., 1964. Chemical composition of Hawaiian lavas. J. Pet. 5, 82–133.
- Maldonado, A., Bohoyo, F., Galindo-Zaldívar, J., Hernández-Molina, F.J., Lobo, F.J., Lodolo, E., Martos, Y.M., Pérez, L.F., Schreider, A.A., Somoza, L., 2014. A model of oceanic development by ridge jumping: opening of the Scotia Sea. Gl. Planet. Change 123. 152-173.
- Martí, J., Geyer, A., Aguirre-Diaz, G., 2013. Origin and evolution of the Deception Island caldera (South Shetland Islands, Antarctica). Bull. Volcanol. 75, 1–18.
- McDonough, W.F., Sun, S.S., 1995. The composition of the Earth. Chem. Geol. 120, 223–253.
- Médard, E., Grove, T.L., 2008. The effect of H2O on the olivine liquidus of basaltic melts: experiments and thermodynamic models. Contrib. Mineral. Petrol. 155, 417–432.
- Michael, P.J., Cornell, W.C., 1998. Influence of spreading rate and magma supply on crystallization and assimilation beneath mid-ocean ridges: evidence from chlorine and major element chemistry of mid-ocean ridge basalts. J. Geophys. Res. 103, 18325–18356.
- Nash, W.M., Smythe, D.J., Wood, B.J., 2019. Compositional and temperature effects on sulfur speciation and solubility in silicate melts. Earth Planet. Sci. 507, 187–198.
- O'Neill, H.S.C., 2021. The thermodynamic controls on sulfide saturation in silicate melts with application to ocean floor basalts. Geophys. Mono. Ser. 266, 177–214.
- O'Neill, H.S.C., Berry, A.J., Mallmann, G., 2018. The oxidation state of iron in Mid-Ocean Ridge Basaltic (MORB) glasses: implications for their petrogenesis and oxygen fugacities. Earth Planet. Sci. Lett. 504, 152–162.
- Panter, K.S., Li, Y., Smellie, J.L., Blusztajn, J., Reindel, J., Odegaard, K., Spicuzza, M.J., Hart, S., 2022. Mantle sources and melting processes beneath East Antarctica: geochemical and isotopic (Sr, Nd, Pb, O) characteristics of alkaline and tholeite basalt from the Earth's southernmost (87° S) volcanoes. Contrib. Mineral. Petrol. 177. 1–26.
- Pearce, J.A., Stern, R.J., Bloomer, S.H., Fryer, P., 2005. Geochemical mapping of the Mariana arc-basin system: implications for the nature and distribution of subduction components. Geochem. Geophys. Geosyst. 6, 1–27.
- Plank, T., 2005. Constraints from Thorium/Lanthanum on sediment recycling at subduction zones and the evolution of the continents. J. Pet. 46, 921–944.
- Plank, T., Forsyth, D.W., 2016. Thermal structure and melting conditions in the mantle beneath the Basin and Range province from seismology and petrology. Geochem. Geophys. Geosyst. 17, 1312–1338.
- Plank, T., Kelley, K.A., Zimmer, M.M., Hauri, E.H., Wallace, P.J., 2013. Why do mafic arc magmas contain ~4wt% water on average? Earth Planet. Sci. 364, 168–179.
- Riley, T.R., Carter, A., Leat, P.T., Burton-Johnson, A., Bastias, J., Spikings, R.A., Tate, A. J., Bristow, C.S., 2019. Geochronology and geochemistry of the northern Scotia Sea: a revised interpretation of the North and West Scotia ridge junction. Earth Planet. Sci. 518, 136–147.
- Roeder, P.L., Emslie, R.F., 1970. Olivine-liquid equilibrium. Contrib. Mineral. Petrol. 29, 275–289.
- Rosenthal, A., Hauri, E.H., Hirschmann, M.M., 2015. Experimental determination of C, F, and H partitioning between mantle minerals and carbonated basalt, CO<sub>2</sub>/Ba and CO<sub>2</sub>/Nb systematics of partial melting, and the CO<sub>2</sub> contents of basaltic source regions. Earth Planet. Sci. Lett. 412, 77–87.
- Rudnick, R.L., McDonough, W.F., Connell, R.J.O., 1998. Thermal structure, thickness and composition of continental lithosphere. Chem. Geol. 145, 395–411.

- Rustioni, G., Audetat, A., Keppler, H., 2021. The composition of subduction zone fluids and the origin of the trace element enrichment in arc magmas. Contrib. Mineral. Petrol. 176, 1–19.
- Saal, A.E., Hauri, E.H., Langmuir, C.H., Perfit, M.R., 2002. Vapour undersaturation in primitive mid-ocean-ridge basalt and the volatile content of Earth's upper mantle. Nature 419, 451–455.
- Schreider, A.A., Schreider, A.A., Galindo-Zaldivar, J., Maldonado, A., Gamboa, L., Martos, Y., Lobo, F., Evsenko, E.I., 2015. Structure of the Bransfield strait crust. Oceanology 55, 112–123.
- Shimizu, K., Saal, A.E., Myers, C.E., Nagle, A.N., Hauri, E.H., Forsyth, D.W., Kamenetsky, V.S., Niu, Y., 2016. Two-component mantle melting-mixing model for the generation of mid-ocean ridge basalts: implications for the volatile content of the Pacific upper mantle. Geochim. Cosmochim. Acta 176, 44–80.
- Smythe, D.J., Wood, B.J., Kiseeva, E.S., 2017. The S content of silicate melts at sulfide saturation: new experiments and a model incorporating the effects of sulfide composition. Am. Min. 102, 795–803.
- Stolper, E., Newman, S., 1994. The role of water in the petrogenesis of Mariana trough magmas. Earth Planet. Sci. Lett. 121, 293–325.
- Stracke, A., 2012. Earth's heterogeneous mantle: a product of convection-driven interaction between crust and mantle. Chem. Geol. 330–331, 274–299.
- Straub, S.M., Layne, G.D., 2003. The systematics of chlorine, fluorine, and water in Izu arc front volcanic rocks: implications for volatile recycling in subduction zones. Geochim. Cosmochim. Acta 67, 4179–4203.
- Taracsák, Z., Mather, T.A., Ding, S., Plank, T., Brounce, M., Pyle, D.M., Aiuppa, A., 2023. Sulfur from the subducted slab dominates the sulfur budget of the mantle wedge under volcanic arcs. Earth Planet. Sci. Lett. 602, 1–14.
- Thomas, R.W., Wood, B.J., 2021. The chemical behaviour of chlorine in silicate melts. Geochim. Cosmochim. Acta 294, 28–42.
- Todt, W., Cliff, R.A., Hanser, A., Hofmann, A., 1996. Evaluation of a <sup>202</sup>Pb-<sup>205</sup>Pb double spike for high-precision lead isotope analysis. In: Hart, S.R., Basu, A., Earth Processes: Reading the Isotopic Code. Geophys. Mono. Ser. 95, 429-437.

- van de Lagemaat, S.H.A., Swart, M.L.A., Vaes, B., Kosters, M.E., Boschman, L.M., Burton-Johnson, A., Bijl, P.K., Spakman, W., van Hinsbergen, D.J.J., 2021. Subduction initiation in the Scotia Sea region and opening of the Drake Passage: when and why? Earth Sci. Rev. 215, 1–25.
- Wallace, P.J., 2005. Volatiles in subduction zone magmas: concentrations and fluxes based on melt inclusion and volcanic gas data. J. Volcanol. Geotherm. Res. 140, 217–240.
- Wallace, P., Carmichael, I.S.E., 1992. Sulfur in basaltic magmas. Geochim. Cosmochim. Acta 56, 1863–1874.
- Wallace, P.J., Edmonds, M., 2011. The sulfur budget in magmas: evidence from melt inclusions, submarine glasses, and volcanic gas emissions. Rev. Mineral. Geochem. 73, 215–246.
- Weaver, S.D., Saunders, A.D., Pankhurst, R.J., Tarney, J., 1979. A geochemical study of magmatism associated with the initial stages of back-arc spreading. Contrib. Mineral. Petrol. 68. 151–169.
- Wiens, D.A., Kelley, K.A., Plank, T., 2006. Mantle temperature variations beneath backarc spreading centers inferred from seismology, petrology, and bathymetry. Earth Planet. Sci. Lett. 248, 30–42.
- Wiens, D.A., Shen, W., Lloyd, A.J., 2023. The seismic structure of the Antarctic upper mantle. Geol. Soc. Lond. Mem. 56.
- Wieser, P.E., Iacovino, K., Matthews, S., Moore, G., Allison, C.M., 2022. VESIcal: 2. A critical approach to volatile solubility modeling using an open source Python3 engine. Earth and Space Science 9, 1–48.
- Workman, R.K., Hart, S.R., 2005. Major and trace element composition of the depleted MORB mantle (DMM). Earth Planet. Sci. Lett. 231, 53–72.
- Yang, A.Y., Langmuir, C.H., Cai, Y., Michael, P., Goldstein, S.L., Chen, Z., 2021.
  A subduction influence on ocean ridge basalts outside the Pacific subduction shield.
  Nat. Com. 12.